Enalapril mitigates aging by targeting antioxidative genes via phosphorylated Smad1/5/9

Wencong Lyu[1†], Haochen Wang[1†], Zhehao Du[1], Ran Wei[1], Jianuo He[1], Fanju Meng[1], Jinlong Bi[1], Lijun Zhang[1], Chao Zhang[2], Yiting Guan[3*] and Wei Tao[1*]

[1]The MOE Key Laboratory of Cell Proliferation and Differentiation, School of Life Sciences, Peking University, Beijing 100871, P. R. China

[2]Kunming Institute of Zoology, Chinese Academy of Sciences, Kunming 650201, P. R. China

[3]Zhanjiang Institute of Clinical Medicine, Central People's Hospital of Zhanjiang, Guangdong Medical University, Zhanjiang 524045, P. R. China

[†]These authors contributed equally to this work

[*]These authors jointly supervised this work

Correspondence:

Wei Tao (weitao@pku.edu.cn)

ABSTRACT

Aging increases the risk of a myriad of chronic diseases, which are expensive and difficult to treat owing to their various risk factors. Repurposing existing anti-aging medications has accelerated the development of therapies aimed at slowing aging. In this study, we revealed that enalapril, a drug widely prescribed for hypertension, can improve both cellular senescence and individual health. Mechanistically, phosphorylated Smad1/5/9 act as pivotal mediators of the anti-aging properties of enalapril. It stimulates downstream genes involved in cell cycle regulation and antioxidative defense, facilitating cell proliferation and diminishing the production of reactive oxygen species (ROS), thus increasing the antioxidative ability of enalapril. At the organismal level, enalapril has been shown to bolster the physiological performance of various organs; it notably enhances memory capacity and renal function and relieves lipid accumulation. Our work highlights the potential of enalapril to augment antioxidant defenses and combat the effects of aging, thereby indicating its promise as a treatment strategy for aging-associated diseases and its use for healthy aging.

INTRODUCTION

Aging is a multifaceted process influenced by numerous factors, and its intricate mechanisms are not yet fully understood. Geroscience is a burgeoning field of study in which researchers hypothesize that aging is a significant risk factor for many chronic diseases. These findings suggest that interventions targeting the mechanisms of aging might delay the onset or slow the progression of these diseases(Kirkland, 2016; Lopez-Otin, Blasco, Partridge, Serrano, & Kroemer, 2023). Cellular senescence, a pivotal indicator of aging, is characterized by irreversible cell cycle arrest triggered by cellular damage or stress(Khosla, Farr, Tchkonia, & Kirkland, 2020). During cellular senescence, cells exhibit increased activity of the lysosomal enzyme senescence-associated β-galactosidase (SA-β-gal), decreased proliferation marker Ki67 signals and increased senescence-associated secretory phenotype (SASP) secretion(Coppe et al., 2008; Dimri et al., 1995).

Senescence is the result of a complex interplay of endogenous and exogenous signaling pathways(Cohen et al., 2022). Currently, the activation of tumor suppressor pathways, such as $p16^{INK4a}$/RB, is deemed essential for senescence-related cessation of proliferation(Baker et al., 2011). The disruption of signaling pathways disrupts tissue homeostasis, leading to proinflammatory responses that are increasingly recognized as fundamental aspects of senescence(Coppe et al., 2008; Shah et al., 2013). Researchers have suggested that the expression of p16 is suppressed by inhibitor of DNA-binding (ID) proteins. The expression of the *ID1* gene is downregulated by transforming growth factor-β (TGF-β), while it is upregulated by BMP-mediated phosphorylated SMAD signaling in various cell types(Hayashi et al., 2016; Liang, Brunicardi, & Lin, 2009). SMADs are crucial transcriptional effector factors responsible for transmitting TGF-β/BMP signals(Urist, 1965). They convey signals from the TGF-β superfamily and homomeric serine/threonine kinases on the cell surface to the nucleus, directly regulating transcriptional programs critical for key events(Miyazono, Maeda, & Imamura, 2005). Numerous studies have shown that the BMP-SMAD signaling pathway can modulate genes involved in the cell cycle, which affects the balance between cell proliferation and senescence(Genander et al., 2014; Hayashi et al., 2016). Phosphorylated SMAD plays a crucial role in the induction and maintenance of

pluripotency, helping maintain tissue homeostasis during aging(Orlowski, 2017). However, dysregulation of BMP signaling during aging can lead to fibrosis, impaired wound healing, or excessive tissue calcification, which are detrimental to tissue function(Lyu et al., 2018; Rahman, Akhtar, Jamil, Banik, & Asaduzzaman, 2015).

Owing to increasing insights into cellular and individual aging, novel aging mechanisms and signaling pathways have been identified, leading to the development of new therapeutic interventions. Senescent cells have recently been targeted in therapy given their substantial impact on aging (Childs et al., 2017). Consequently, eliminating senescent cells through pharmacological interventions, known as "senolytics", may delay the onset or slow the progression of age-related diseases and enhance physiological function(Childs et al., 2017). Research has proven that specific senolytic drugs, such as dasatinib and quercetin, can eliminate senescent cells, reverse aging phenotypes and increase the survival rate of mice(Xu et al., 2018; Zhu et al., 2015). However, the current senolytics are not universally effective across different cell types and display inconsistent sensitivities, thereby limiting their broad application(Yousefzadeh et al., 2018; Zhu et al., 2016). In addition to senolytics, researchers have explored pharmacological interventions that aim to ameliorate or reverse aging phenotypes without the need to eliminate senescent cells. This included both the repurposing of existing medications and the development of new ones(Bharath et al., 2020; Harrison et al., 2014). However, repurposing is particularly attractive due to its cost-effectiveness; these drugs have already undergone rigorous safety evaluations, allowing for quicker implementation in new contexts. For example, drugs such as metformin, which is typically used to treat type 2 diabetes, and rapamycin, an immunosuppressant, have shown promise in reducing aging phenotypes and extending the lifespan(Bharath et al., 2020; Harrison et al., 2009). This strategy is an innovative pharmacological intervention in which existing compounds target the aging process.

In this study, we employed a drug repurposing strategy to evaluate the anti-aging potential of several FDA-approved drugs and identified enalapril as a promising candidate. Our investigation revealed that enalapril increases pSmad1/5/9 levels, which in turn upregulates key downstream genes involved in cell cycle regulation and antioxidative defense, thereby improving cell proliferation, reducing inflammation, and

decreasing reactive oxygen species (ROS) levels. Our findings confirmed the anti-aging mechanism of enalapril at both the cellular and organismal levels. Enalapril has the ability to delay the aging of various organs, with notable effects on the brain, kidney, and liver. Furthermore, treating aged mice with enalapril improved spatial memory and anxiety behavior, alleviated lipid accumulation, and slowed kidney aging. Taken together, the potential of enalapril to extend the lifespan and ameliorate age-related diseases makes it a compelling candidate for research and development in the field of anti-aging therapeutics.

MATERIALS AND METHODS

Cell culture

IMR90 cells were cultured in DMEM (Gibco, C11995500) supplemented with 10% fetal bovine serum (Cellmax, SA111) and 1% non-essential amino acids (Gibco, 11140050) at 37°C and 5% CO_2. When the cell density in the in vitro culture reached 80–90% (usually within 2 or 3 days), cell passage was performed.

Drug preparation and addition

Enalapril (MCE, HY-B0331) was dissolved in DMSO to prepare a 10 mM stock solution. When used, it was diluted to 10 μM in the culture medium. After the cells adhered to the surface, enalapril was added for treatment, and RNA and protein were collected for analysis. Recombinant BMP4 protein (MCE, HY-P7007) was dissolved in sterile ddH_2O to prepare a 100 μg/mL stock solution. When used, it was diluted to 50 ng/mL in the culture medium and added to the cells. The BMP receptor inhibitor (LDN193189, MCE, HY-12071) was dissolved in sterile ddH_2O to prepare a 1 mM stock solution. When used, it was diluted to 1 μM or 0.5 μM in the culture medium. The ID inhibitor (Pimozide, MCE, HY-12987) was dissolved in DMSO to prepare a 10 mM stock solution. When used, it was diluted to 5 μM in the culture medium. After the cells adhered to the surface, drugs were added for a 3-day treatment, and samples were collected for analysis.

Senescence-associated β-galactosidase (SA-β-gal) Staining

SA-β-gal staining was performed using a Senescence β-Galactosidase Staining Kit (Sigma–Aldrich, CAS0030). Briefly, 0.6×10^5 cells were seeded in a 6-well plate. The cells were fixed with fixation buffer and incubated at room temperature for 10 minutes. After the cells were washed three times with PBS, the prepared staining mixture was added to the 6-well plate, and the plate was incubated at 37°C overnight. The stained cells were observed and photographed under a microscope.

Western blot

Proteins were extracted using TRIzol reagent (Invitrogen, 15596018CN) and dissolved in 1% SDS, after which SDS–PAGE was performed. The samples were transferred to nitrocellulose membranes and incubated with 5% skimmed milk at room temperature for 30 minutes. The primary antibodies were incubated overnight at 4°C, followed by three washes with PBST. The membranes were then incubated with secondary antibody at room temperature for two hours. The band signals were visualized using an Odyssey Infrared Imaging System (Odyssey, LI-COR).

RT-qPCR

Total RNA from cultured cells was extracted using TRIzol reagent (Invitrogen, 15596018CN) according to the manufacturer's instructions. The DEPC-treated water-dissolved RNA was subsequently reverse transcribed into cDNA using the HiScript III All-in-one RT SuperMix Perfect for qPCR (Vazyme, R333) following the product manual. The cDNA levels of specific primers were analyzed using the LightCycler® 96 qPCR system (Roche), and the results were normalized to those of β-actin. The primers used in this analysis are listed in Table S1.

RNA-seq and data processing

Total RNA was extracted using TRIzol reagent (Invitrogen, 15596018CN) following the manufacturer's instructions. The extracted total RNA was then sent to Novogene for subsequent cDNA library construction. The library was sequenced with paired-end reads on the Illumina HiSeq PE150 platform.

For data processing, FastQC (version 0.11.5) software was first used for data quality control. Raw paired-end sequencing reads were trimmed by Trim Galore (version 0.6.10) software to remove adapter sequences and low-quality reads. The high-quality RNA-seq reads were mapped to the hg38/mm10 genome using HISAT2 (version 2.2.1) software(Kim, Paggi, Park, Bennett, & Salzberg, 2019). SAMtools (version 1.17) software was then used to convert the generated SAM files to bam files(Li et al., 2009). To qualify gene expression, the number of reads mapped to each gene was counted using featureCounts (version 2.0.1) software(Liao, Smyth, & Shi, 2014). Differentially expressed genes (DEGs) were calculated by R package DESeq2 (version 1.34.0)(Love, Huber, & Anders, 2014) with the cutoff values of Benjamini-Hochberg adjusted p-value < 0.05 and $|\log_2(\text{fold change})| > 0.5$. The gene expression count matrix was converted into the reads per kilobase per million mapped reads (RPKM) matrix, followed by Z score normalization for visualization.

CUT&Tag and data processing

For the CUT&Tag experiments, 8×10^5 cells were processed using the CUT&Tag Kit (Vazyme, TD903). The cells were collected and incubated with ConA beads and then mixed with the primary antibody pSmad1/5/9 (CST, #13820) overnight at 4°C. After incubation with the secondary antibody for one hour, the cells were further incubated with pA/G-Tnp for one hour. The transposase was then activated for DNA fragmentation. Following DNA extraction, library amplification and purification were performed. The libraries were sequenced using paired-end reads on the Illumina HiSeq PE150 platform.

For data processing, raw CUT&Tag data was trimmed using Trim Galore (version 0.6.10) software, and the clean reads were mapped to the human reference genome hg38 using Bowtie2 (version 2.5.1) software(Langmead & Salzberg, 2012) with the following parameters: “--very-sensitive --no-mixed --no-discordant -I 10 -X 1000”. The SAM files were transformed into bam files via SAMtools (version 1.17) software(Li et al., 2009). The CUT&Tag peaks were performed using the MACS2 (version 2.2.8) with the default parameters(Zhang et al., 2008). Differential peaks were calculated using the R package DiffBind (version 3.4.11) with the cutoff values of adjusted p-value < 0.05

163 and |$\log_2$(fold change)| > 0.5 and annotated using the R package ChIPpeakAnno
164 (version 3.28.0)(Lihua, Claude, & Nathan, 2010). To visualize the CUT&Tag signal,
165 the reads per kilobase per million mapped reads (RPKM) were calculated in each 50-
166 bp bin size using DeepTools (version 3.5.2) software(Ramirez, Dundar, Diehl, Gruning,
167 & Manke, 2014), and the RPKM matrix was normalized using the Z score algorithm.

168 **ChIP-qPCR**

169 At room temperature, approximately 2 × 10^6 IMR90 cells were cross-linked with 1%
170 paraformaldehyde for 10 minutes. The cross-linking reaction was stopped by adding
171 0.125 M glycine for 6 minutes. The cells were then harvested and lysed on ice in nuclear
172 lysis buffer (50 mM Tris-Cl, 10 mM EDTA, 1% SDS, and protease inhibitors).
173 Chromatin immunoprecipitation (ChIP) was performed using a Bioruptor (Diagenode)
174 to shear the chromatin. Fragmented chromatin (25 μg) was immunoprecipitated with 5
175 μg of anti-pSmad1/5/9 antibody (CST, #13820) or anti-rabbit IgG (Abcam, ab171870).
176 The immunoprecipitated DNA was quantified via RT-qPCR. The amount of DNA in the
177 immunoprecipitates was calculated as a percentage relative to 10% of the input
178 chromatin. All ChIP-qPCR-related primers are available in Table S2.

179 **Immunofluorescence**

180 The slides were washed twice in PBS, fixed with 4% PFA for 10 minutes, and washed
181 again three times with PBS. Subsequently, permeabilization was performed via
182 incubation with 0.5% Triton X-100 for 10 minutes, followed by three additional washes
183 with PBS. Next, blocking was performed with 1% BSA, and after blocking, the slides
184 were washed three times with PBS. The primary antibody was then diluted at a ratio of
185 1:500 in PBST (PBS + 0.1% Tween 20) and incubated overnight at 4°C. Afterward, the
186 slides were washed four times with PBST, with each wash lasting 5 minutes. The
187 secondary antibody was diluted at a ratio of 1:500 in PBST (1 × PBS + 0.1% Triton X-
188 100) and incubated at room temperature for 1–1.5 hours. After three washes with PBST,
189 a final wash with PBS was conducted. DAPI was diluted to a final concentration of 1–
190 2 ng/μL and incubated at room temperature for 3–5 minutes. Following three washes
191 with PBS and one wash with ddH_2O, the slides were sealed with Fluoromount-G®
192 (SouthernBiotech, 0100-010) and covered with a coverslip.

193 **Lentiviral production and viral transduction**

194 First, the pLKO.1 empty vector or vectors encoding shRNAs targeting *ID1* or *ID2*
195 (Table S3), along with the assistant plasmids psPAX2 and pMD2.G, were cotransfected
196 into HEK293T cells. After 18 h of transfection, the medium was replaced with DMEM
197 supplemented with 30% complement-inactivated FBS, and viral supernatants were
198 collected after 24 h and 48 h of transfection. When IMR90 cells reached 70%
199 confluence, they were infected with the packaged virus with 5 μg/mL polybrene (MCE,
200 HY-K1057). At 36–48 hours after infection, successfully transduced cells were selected
201 via treatment with 1 μg/mL puromycin (M&C Gene Technology, MA009) for 24–36
202 hours.

203 **Detection of Reactive Oxygen Species (ROS)**

204 IMR90 cells were harvested from a 6-well plate. After the cells were washed, the ROS-
205 sensitive fluorescent probe 2',7'-dichlorofluorescin diacetate (DCFH-DA, MCE, HY-
206 D0940) was used for detection. A 10 mM stock solution of DCFH-DA was prepared by
207 dissolving it in anhydrous DMSO. This stock solution was subsequently diluted in
208 serum-free DMEM to obtain a 10 μM working solution of DCFH-DA. The samples
209 were incubated with the DCFH-DA probe at 37°C for 30 minutes. After incubation, the
210 samples were washed to remove excess probe. The fluorescence intensity was measured
211 via a fluorescence microscope. The fluorescence intensity corresponds to the level of
212 ROS present in the sample.

213 **Mice feeding**

214 All the mouse experiments were approved by the Institutional Animal Care and Use
215 Committee of Peking University. Twelve-month-old C57BL/6 mice (purchased from
216 Wukong Biotech Co., Ltd.) were housed in a specific pathogen-free (SPF) animal
217 facility under controlled environmental conditions with a temperature range of 20–25°C,
218 55±10% humidity, and a 12-h light/dark cycle. The mice had ad libitum access to food
219 and water. A daily dosage of 30 mg/kg of enalapril was dissolved into the mice's
220 drinking water. Four to ten mice were included in each group.

221 **Forelimb grip strength test**

The mice were placed on a grip strength meter, and their tails were gently pulled to allow them to grasp the pull bar with their forelimbs. The grip strength meter readings were recorded at the point of maximum force exerted by each mouse. The measurements were repeated multiple times to ensure reliable and consistent results.

Rotarod fatigue test

The mouse was placed on the rotarod, and rotation was initiated. The device was set to an accelerating mode that increased from 4 to 40 revolutions per minute over 300 seconds. The time at which each mouse fell off or lost balance was recorded. The test was repeated multiple times to assess the endurance and motor performance of the mice.

Y-maze test

The Y-maze consists of three opaque arms arranged at 120° angles relative to each other. The mice were placed in the central position of the maze and allowed to explore the three arms freely for 10 minutes. Each consecutive entry into one of the three arms was defined as spontaneous alternation behavior. The total number of arm entries and the number of spontaneous alternations were recorded. The percentage of spontaneous alternation behavior was then calculated.

Open field test

The mice were removed from their cages and placed in an open field, with the central area designated. The mice were allowed to move freely within the open field for 10 minutes, and the number of times that they crossed the central area was recorded.

Mouse serum extraction and analysis

After the mice were anesthetized, blood (approximately 1 mL per mouse) was collected from the eyeballs. The blood was allowed to clot and settle at room temperature. The mixture was then centrifuged at 3,000 rpm for 20 minutes, and the upper clear layer, which was the serum, was collected. The serum was subsequently subjected to biochemical assays, including ALT, CREA, LDH, TG, LDL, and HDL tests.

Mouse tissue extraction

After the mice were euthanized, they were perfused with prechilled PBS until no blood was expelled. The heart, liver, spleen, kidney, brain, and muscle tissues were harvested. A portion of each tissue sample was used for RNA and protein extraction for sequencing and Western blot analysis, respectively, while another portion was fixed in 4% paraformaldehyde (PFA). The tissues were then subjected to either frozen or paraffin embedding. Various staining techniques, including β-galactosidase (β-gal) staining, periodic acid-Schiff (PAS) staining, Congo red staining, Sirius red staining, Oil Red O staining, and hematoxylin and eosin (H&E) staining, were performed.

Pathway enrichment analysis

Gene Ontology (GO) enrichment analysis was performed with Metascape(Zhou et al., 2019), and gene set enrichment analysis (GSEA) was performed with the R package ClusterProfiler (version 4.2.2)(Wu et al., 2021). Pathways with p values < 0.05 were considered significantly enriched. Representative terms were visualized with the ggplot2 (version 3.3.6) R package and ComplexHeatmap (version 2.10.0) R package(Gu, 2022).

Statistical analysis

The data are expressed as means ± SEMs. The data were analyzed via a two-tailed unpaired Student's t test. A p value < 0.05 was considered statistically significant.

RESULTS

Enalapril restrains cellular replicative senescence.

To identify drugs that are capable of delaying cellular senescence, we established an in vitro replicative senescence model using primary human embryonic lung fibroblasts (IMR90). Compared with young cells, long-term-cultured IMR90 cells presented a characteristic senescence phenotype, characterized by increased SA-β-gal staining, increased expression of the cell cycle arrest factors p16 and p21, and reduced expression of the proliferation marker Ki67 (**Fig. S1A-C**). Additionally, the release of SASP factors that significantly alter the cellular microenvironment, including the well-described factors *IL-1β*, *IL-6*, and *CXCL10,* has also been reported to increase the degree of

277 senescence (**Fig. S1D**).

278 Employing a drug repurposing strategy, we discovered that enalapril, an
279 antihypertensive medication, delayed senescence. Notably, enalapril treatment at
280 various concentrations reduced SA-β-gal staining and increased Ki67 positivity in
281 IMR90 cells (**Fig. 1A-B, D-E**). Western blot analysis confirmed a decrease in the aging
282 markers p16 and p21 with the optimal effect of 10 μM enalapril (**Fig. 1C**). To further
283 analyze the effects of enalapril on transcriptome dynamics upon senescence entry,
284 RNA-seq was performed across enalapril-treated cells at different concentrations. In
285 general, we found that the expression of SASP genes decreased significantly (**Fig. 1F**).
286 The expression of cell cycle arrest factors typically increased during senescence;
287 however, the expression of these factors decreased after exposure to enalapril, whereas
288 the expression of cell cycle genes related to cell proliferation increased upon treatment
289 with enalapril at the optimal concentration of 10 μM (**Fig. 1F**). We therefore treated the
290 cells with 10 μM enalapril via RT-qPCR and detected that many prominent SASP genes,
291 such as *IL-1β and IL-6*, were significantly reduced compared with those in the control
292 (**Fig. 1G**). Moreover, enalapril treatment increased the cell growth rate and delayed the
293 transition to the growth arrest phase (**Fig. 1H**). Our comprehensive analysis underscores
294 enalapril's potential as an anti-senescence agent, warranting further exploration for its
295 role in combating cellular senescence.

296 **The function of enalapril depends on phosphorylated Smad1/5/9.**

297 Given the potential of enalapril to decelerate senescence, we screened several important
298 targets of the aging-related pathway to identify the underlying mechanism of
299 senescence entry. We found that enalapril notably elevated the phosphorylation level of
300 Smad1/5/9 without affecting Smad2/3 phosphorylation, suggesting a possible role for
301 the BMP-pSmad1/5/9 pathway (**Fig. 2A, Fig. S2A**). To validate the pathway alterations
302 in the gene expression profile, GSEA confirmed that enalapril treatment increased BMP
303 signaling (**Fig. 2B**). Concurrently, the level of the Smad4 protein, which is required for
304 pSmad1/5/9 to enter the nucleus, also increased, suggesting that enalapril might
305 facilitate the nuclear entry of pSmad1/5/9 and modulate downstream genes (**Fig.
306 2A**)(Guglielmi et al., 2021; Senft, Bikoff, Robertson, & Costello, 2019). To further

307 assess the impact on gene regulation, we employed CUT&Tag analysis of pSmad1/5/9
308 and found that enalapril treatment increased the pSmad1/5/9 binding signals at the
309 transcription start site (TSS) regions (**Fig. 2C**).

310 To explore the potential role of pSmad1/5/9 in anti-senescence mechanisms, we
311 experimentally manipulated its protein levels by supplementing with BMP4 to increase
312 pSmad1/5/9 levels or employing the BMP receptor inhibitor LDN193189 (LDN) to
313 reduce it. Our findings revealed that BMP4 increased pSmad5 levels, which correlated
314 with decreased p16 and p21, reduced β-gal staining and increased Ki67 positivity,
315 indicating a mitigated senescent phenotype (**Fig. S2B-D**). In contrast, when cells were
316 treated with the BMP receptor inhibitor, the changes in pSmad1/5/9 levels and
317 senescence markers were completely reversed, highlighting the accelerated progression
318 of senescence under the influence of the BMP receptor inhibitor (**Fig. S2E-G**).

319 Encouraged by the association between increased pSmad1/5/9, we tested whether
320 pSmad1/5/9 serves as an intermediary in the anti-senescence effects of enalapril by
321 combining LDN with enalapril. RNA-seq analysis revealed that LDN upregulated
322 SASP genes and downregulated cell cycle genes. On the basis of these findings, the
323 subsequent addition of enalapril did not reverse these changes, which suggests that the
324 anti-senescence function of enalapril relies on pSmad1/5/9 (**Fig. 2D**). Furthermore,
325 western blot results also revealed that in the presence of LDN, neither enalapril nor
326 BMP4 restored Smad1/5/9 phosphorylation or the expression of p16 and p21 (**Fig. 2E**).
327 Similarly, β-gal and Ki67 staining also revealed that enalapril failed to counteract LDN-
328 induced deterioration (**Fig. 2F, G**). Collectively, these results indicate that elevated
329 pSmad1/5/9 could increase the expression of critical genes, thereby exerting a potent
330 anti-senescence effect.

331 **pSmad1/5/9 modulates the cell cycle and SASP secretion by upregulating ID1.**

332 The ID family, which is recognized as a key downstream target of pSmad1/5/9, serves
333 as a biomarker for Smad1/5/9 phosphorylation levels(Genander et al., 2014; Hayashi et
334 al., 2016; Ramachandran et al., 2018; Sun et al., 2022; Ying, Nichols, Chambers, &
335 Smith, 2003). Coincidentally, we found that ID1 was the top-ranked transcription factor
336 that pSmad1/5/9 bound to its promoter region via CUT&Tag analysis after enalapril

treatment (**Fig. 3A**). Moreover, IGV analysis confirmed that enalapril significantly increased pSmad1/5/9 enrichment at the *ID1* promoter (**Fig. 3B**). Simultaneously, the expression levels of both *ID1* and *ID2* were elevated (**Fig. 3C, D**). Conversely, inhibiting pSmad1/5/9 with LDN led to decreased *ID1* and *ID2* levels, confirming the regulatory link between pSmad1/5/9 and the ID family (**Fig. 3E**). This finding indicated that the ID family was indeed a downstream gene regulated by pSmad1/5/9, and the increase in ID1 induced by enalapril further confirmed that enalapril could upregulate pSmad1/5/9 levels, thereby affecting the expression of downstream genes.

Prior studies have indicated that the ID family can suppress p16 and p21 expression, thus inhibiting cell cycle arrest and delaying cellular senescence(Hayashi et al., 2016; Lyden et al., 1999; Ying et al., 2003). This prompted us to examine ID protein expression during senescence, where we observed a decrease in ID1 and ID2 levels (**Fig. S3A**). The knockdown of *ID1* and *ID2* via shRNA or an ID1 inhibitor resulted in a decreasing trend of ID1 or ID2 expression and a significant increase in p16 and p21 expression (**Fig. 3F, I**). In addition, while β-gal increased the proportion of positively stained cells, the Ki67 proliferation signal decreased nearly fourfold after the knockdown of *ID1* or *ID2*, resembling the changes observed during senescence (**Fig. S3B, C)**. Given that enalapril reduced SASP factors while LDN increased them, we investigated whether ID1, which acts as a transcriptional repressor downstream of pSmad1/5/9, could modulate SASP expression. Indeed, the expression of traditional SASP factors, such as *IL1β* and *IL6*, which decrease with enalapril treatment, significantly increased after *ID* knockdown (**Fig. 3G**). By overlapping the genes downregulated by enalapril with those upregulated upon *ID* knockdown, several SASP genes, as well as *CDKN2A* and *CDKN2B,* were identified (**Fig. 3H**). Consistent with these findings, we found that SASP factor expression also increased in *ID* knockout mouse bone marrow cells in previously reported data (**Fig. S3E**)(Fei et al., 2023). Importantly, *ID* knockdown did not affect pSmad1/5/9 levels, confirming that ID is a downstream effector of pSmad1/5/9, influencing the expression of genes such as p16, p21, and SASP-related genes (**Fig. 3J**).

After validating the prosenescence effects of *ID1* or *ID2* through ID1 knockdown or the use of small molecule inhibitors, we next examined whether the anti-senescence

368 effects of enalapril are mediated by ID proteins. The continued addition of enalapril to
369 these *ID*-knockdown cells did not significantly alter β-gal or Ki67 signals compared
370 with those in the *ID*-knockdown group without enalapril, implying that the benefits of
371 enalapril may be ID dependent (**Fig. 3K-L, Fig. S3D**). Taken together, these findings
372 indicate that enalapril elevates pSmad1/5/9 levels, which in turn upregulate *ID1*
373 expression. This dual action has two key implications: first, it confirms that enalapril
374 can modulate the expression of pSmad1/5/9 downstream genes. Second, by
375 upregulating ID1, enalapril can suppress the expression of p16, p21, and SASP-related
376 genes, thereby potentially restoring cell proliferation and reducing the expression of
377 inflammatory factors. These findings suggest that the anti-senescence mechanism of
378 enalapril involves the pSmad1/5/9-ID1 axis, highlighting a novel pathway for its
379 therapeutic effects on aging.

380 **Enalapril has antioxidative effects through pSmad1/5/9.**

381 Since an increase in pSmad1/5/9 after enalapril treatment was observed and
382 pSmad1/5/9 is a transcription factor, to understand the in-depth mechanism of enalapril
383 regulation, we further explored the downstream genes of pSmad1/5/9. Analysis of
384 CUT&Tag-upregulated peaks after enalapril treatment revealed that enalapril treatment
385 led to enrichment of pSmad1/5/9 in the GO pathway associated with DNA replication,
386 the cell cycle and the oxidative stress response, all of which are crucial for cell growth
387 (**Fig. 4A**). Moreover, transcriptome analysis revealed that the genes whose expression
388 increased after enalapril treatment were also enriched in pathways related to the
389 response to oxidative stress (**Fig. 4A**). Notably, genes upregulated by enalapril in
390 response to oxidative stress included antioxidative enzymes, electron transport chain
391 components and lipid oxidation inhibitors, with a significant increase in pSmad1/5/9 at
392 their TSS regions (**Fig. 4B, C**). Specifically, we also examined the promoter regions of
393 antioxidative genes, such as the antioxidative enzyme *PRDX5* and the lipid oxidation
394 inhibitor *TXN*, and found increased pSmad1/5/9 enrichment along with upregulated
395 gene expression (**Fig. 4D, F-H**). During cellular senescence, a decrease in these
396 antioxidative genes exacerbates oxidative stress, reduces energy metabolism, and
397 increases lipid oxidation, leading to the release of inflammatory cytokines (**Fig.**

398 **4E**)(Coppe et al., 2008).

399 It has been reported that changes in the expression of antioxidative genes can affect
400 the ROS level of cells; thus, we then used DCFH-DA probes to detect ROS levels in
401 cells(Coppe et al., 2008). The results revealed that cellular senescence increased ROS,
402 whereas enalapril slowed the increase in ROS, indicating its ability to upregulate
403 antioxidative genes and reduce ROS, thus affecting cellular senescence (**Fig. 4I**).
404 Importantly, the continued addition of BMP receptor inhibitors reversed the beneficial
405 effects of enalapril on ROS and decreased pSmad1/5/9 enrichment of these
406 antioxidative genes (**Fig. 4G, I**). Collectively, these results reinforce the notion that
407 enalapril promotes the upregulation of antioxidative genes through pSmad1/5/9,
408 reduces ROS levels and alleviates oxidative stress, thus playing a crucial role in
409 delaying senescence.

410 **Enalapril upregulates pSmad1/5/9 and improves physiological function in mice.**

411 Enalapril, which is known for its anti-senescence potential, was further investigated for
412 its impact at the organ and individual levels in 12-month-old mice (**Fig. 5A**). After
413 continuous feeding at a dosage of 30 mg/kg/day for 3 months, we conducted a
414 comprehensive RNA-seq analysis of six key organs—brain, kidney, liver, heart, muscle,
415 and spleen—to assess the impact of enalapril on the transcriptome. We found that
416 enalapril induced organ-specific gene expression changes, thereby affecting the
417 physiological functions of these genes. Moreover, GSEA revealed upregulated
418 pathways related to forebrain and kidney development, long-chain fatty acid
419 metabolism and other processes, indicating that enalapril has a beneficial effect on
420 organ functions (**Fig. S4A**). Additionally, enalapril reduced the expression of SASP
421 factors in multiple organs, particularly the CCL, CXCL, and MMP families (**Fig. 5B**).
422 Serum SASP array analysis also revealed a decrease in the secretion of certain SASP
423 proteins, such as CCL6, CCL11, CXCL13, IGFBP-1, and MMP3, suggesting that
424 enalapril has anti-inflammatory effects in mice (**Fig. 5C**).

425 Given the known upregulation of pSmad1/5/9 levels and antioxidative genes in
426 cellular studies by enalapril, we measured Smad1/5/9 phosphorylation and the
427 expression of the antioxidative genes *Txn1*, *Txn2*, and *Prdx5* in the tested organs. We

428 observed increased pSmad1/5/9 levels, especially in the brain, kidney and liver, along
429 with upregulated *Id1* and antioxidative genes, notably *Txn1* and *Txn2* (**Fig. 5D, Fig.**
430 **S4B**). Further analysis of BMP signaling and antioxidative stress-related pathways in
431 these organs revealed increased gene expression after enalapril treatment, indicating the
432 activation of this pathway (**Fig. 5E**). These findings align with our cellular findings,
433 implying that enalapril may enhance the pSmad1/5/9-antioxidative gene axis to
434 increase organ physiological function and delay individual aging.

435 **Enalapril alleviates aging-related behavior in naturally aged mice.**

436 Building on our finding of pSmad1/5/9 activation and antioxidative genes upregulation
437 in multiple organs, we further investigated the broader phenotypic effects of enalapril
438 in mice. After three months of enalapril feeding, behavioral experiments, serum tests,
439 and tissue section staining were performed. Notably, enalapril had no significant effect
440 on body weight in the mice, suggesting that the drug has no overt toxic side effects (**Fig.**
441 **6A**). However, enalapril improved the decrease in age-related mobility, as evidenced
442 by increased grip strength and extended time in the rotarod fatigue experiments,
443 suggesting increased muscle strength and endurance (**Fig. 6D, E**).

444 During the aging process, the brain undergoes varying degrees of functional
445 decline. To assess the impact of enalapril on brain function, we conducted Y-maze and
446 open field tests. The Y-maze, which is frequently employed to assess short-term
447 memory in mice by measuring spontaneous alternation as a marker of spatial working
448 memory, indicates notable improvements. Under normal circumstances, mice prefer to
449 explore new maze branches rather than return to previously visited branches. Several
450 brain regions, including the hippocampus, septum, basal forebrain, and prefrontal
451 cortex, contribute to this task, and the age-related decline in spontaneous alternation
452 ability in mice is associated with degeneration or lesions in brain regions such as the
453 hippocampus(Radulescu, Cerar, Haslehurst, Kopanitsa, & Barnes, 2021). Enalapril
454 promoted a substantial increase in the rate of spontaneous alternation in the mice,
455 indicating enhanced spatial memory (**Fig. 6B, C**). As aging progresses, anxiety-like
456 behaviors often increase with age in mice(Radulescu et al., 2021). The open-field test,
457 a valuable tool for assessing autonomous and exploratory behaviors in new

environments, demonstrated that enalapril increased the number of central area crossings, suggesting a reduction in aging-related anxiety (**Fig. 6F, G**). In conclusion, these results suggest that enalapril has the potential to mitigate the deterioration of various behavioral aspects associated with aging, including endurance, spatial memory and anxiety.

Enalapril ameliorates aging-related pathological changes in aged mice.

The results of these behavioral tests provided valuable insights. To further explore the effects of enalapril on pathological changes, our investigation was extended to serum analyses. This comprehensive analysis encompassed the evaluation of vital organ function, including the liver, kidneys, and heart, as well as an assessment of lipid content, specifically triglycerides (TGs), low-density lipoprotein cholesterol (LDL), and high-density lipoprotein cholesterol (HDL). After enalapril administration, there was no significant change in the serum alanine transaminase (ALT) level, indicating that no liver toxicity from enalapril occurred (**Fig. 6H**). Moreover, the level of creatinine (CREA), a key marker of kidney function, was significantly decreased in enalapril-treated mice, indicating potential functional recovery and improvement of renal function (**Fig. 6I**). A heart health indicator, lactate dehydrogenase (LDH), was also reduced, indicating a positive cardiac effect of enalapril (**Fig. 6J**). These findings underscore the multifaceted effects of enalapril on various physiological parameters, emphasizing its potential as a therapeutic intervention in aging-related conditions.

The transcriptomic data from the enalapril treatment group revealed an increase in long-chain fatty acid metabolism in the liver, suggesting that enalapril may play a positive role in lipid metabolism (**Fig. S4A**). Accordingly, we analyzed serum lipid levels in enalapril-treated mice. Typically, aging leads to a decline in lipid metabolism in the serum, causing an accumulation of triglycerides (TGs) and low-density lipoprotein (LDL) and a decrease in high-density lipoprotein (HDL), contributing to oxidative stress and conditions such as hyperlipidemia and fatty liver(A. A. Johnson & Stolzing, 2019). Following enalapril treatment, the mice presented significant reductions in TG and LDL levels and a noticeable increase in HDL levels (**Fig. 6K-M**). These results suggest that enalapril has the potential to increase lipid metabolism in

488 aged mice, thereby mitigating the increase in blood lipid levels.

489 To evaluate the improvements in the aging process induced by enalapril in various
490 organ systems, we conducted pathological examinations of mouse tissues. A decrease
491 in β-gal staining was observed in the brain, liver and spleen of enalapril-treated mice,
492 suggesting a delay in organ aging (**Fig. 6N**). Given the effects of enalapril on brain
493 function, we further examined pathological markers in the brain. Periodic acid-Schiff
494 (PAS) staining, which is indicative of glycogen deposition, revealed a significant
495 reduction in glycogen near the hippocampus (**Fig. 6O**). Congo red staining, which
496 detects amyloid protein deposition, also revealed reduced staining in the cerebral cortex
497 (**Fig. 6P**). In the kidney, Sirius red staining, which highlights abnormal collagen fibers
498 or fibrosis, revealed significant red staining around blood vessels in control mice.
499 However, this staining was noticeably reduced in the kidneys of the mice treated with
500 enalapril (**Fig. 6Q**). These findings suggest that enalapril has a beneficial effect on
501 fibrosis in the kidneys of aged mice, which aligns with the observed improvement in
502 plasma creatinine levels (**Fig. 6I**). Furthermore, analysis of spleen, kidney and liver
503 sections from enalapril-treated mice revealed a reduction in Oil Red O staining, with
504 the kidneys and liver showing the most significant changes (**Fig. 6R**). This finding
505 aligned with the consistent decrease in lipid-related molecular content in plasma,
506 indicating that enalapril has a role in reducing age-related lipid accumulation (**Fig. 6K-**
507 **M**). Hematoxylin and eosin (H&E) staining of the liver revealed a decrease in cavities
508 and increased tissue density in mice treated with enalapril, suggesting its role in
509 enhancing liver cell proliferation and regeneration (**Fig. 6S**).

510 In summary, enalapril significantly mitigated multiple pathological markers
511 associated with aging, including lipid droplets, amyloid, glycogen deposition, and
512 fibrosis, in the brain, kidneys, liver, heart and spleen of aged mice. These
513 comprehensive improvements contribute to an overall amelioration of their aging status.

514 DISCUSSION

515 Since the early 2000s, the National Institutes of Health (NIH) has been pioneering the
516 Interventions Testing Program (ITP), an initiative aimed at harnessing existing drugs or
517 small molecules to decelerate the aging process(Harrison et al., 2009; Nadon et al., 2008;

Strong et al., 2016). This approach repurposes established medications for novel uses, maximizing the potential of known compounds. It has accelerated the transition of anti-aging therapies from discovery to clinical application, ensures their safety and bolsters a comprehensive anti-aging drug screening strategy.

In our study, we discovered that enalapril, a commonly prescribed ACE inhibitor for hypertension, has significant anti-aging effects at both the cellular and organismal levels (**Fig. 7**). Enalapril demonstrated a notable ability to attenuate aging-related physiological decline across multiple organs, including the brain, kidneys, and liver. This finding suggests its potential to reduce the risk of disease across multiple organs, slow the overall aging process and extend both the healthspan and lifespan of mice. This observation aligns with previous reports on the lifespan-extending effects of other ACE inhibitors, such as captopril, which have been shown to increase longevity in organisms such as *C. elegans* and mice(Egan et al., 2024; Kumar, Dietrich, & Kornfeld, 2016; Strong et al., 2022). However, our screening process revealed that enalapril outperformed captopril and other antihypertensive drugs in ameliorating senescent phenotypes, although captopril and other antihypertensive drugs also exhibited the ability to delay senescence. These findings indicate that enalapril may have unique or more potent mechanisms of action that contribute to its anti-aging effects, warranting further mechanistic studies to better understand its molecular targets.

Mechanistically, our data revealed that enalapril enhances the phosphorylation of Smad1/5/9, a critical signaling pathway that regulates various cellular processes, including cell proliferation and the oxidative stress response. Phosphorylation of Smad1/5/9 facilitates its nuclear translocation, where it acts as a transcriptional regulator to upregulate downstream genes, such as those involved in cell cycle regulation and antioxidative responses. These findings suggest that the ability of enalapril to modulate the pSmad1/5/9 pathway contributes to its protective effects against oxidative stress, a well-established hallmark of aging. By reducing ROS levels and promoting cell proliferation, enalapril effectively delays the progression of cellular senescence and organismal aging. This finding not only highlights the potential of phosphorylated Smad1/5/9 as a therapeutic target for anti-aging interventions but also reveals a novel antioxidative mechanism of enalapril action.

Several FDA-approved drugs have been repurposed for anti-aging applications, demonstrating a wide range of mechanisms and effects. These include rapamycin, metformin, and NAD+ precursors. For example, rapamycin, which was originally used as an immunosuppressant to prevent organ transplant rejection, inhibits the mTOR pathway, which is associated with cell growth and metabolism(S. C. Johnson, Rabinovitch, & Kaeberlein, 2013). It extends the lifespan of mice and shows potential anti-aging effects across various species(Harrison et al., 2009). Compared with other repurposed anti-aging drugs, enalapril offers distinct advantages because of its unique mechanism of action. As an ACE inhibitor, enalapril inherently targets the renin–angiotensin system, providing vascular protection(Schmieder, Hilgers, Schlaich, & Schmidt, 2007; Yamamoto & Rakugi, 2021). Compared with repurposed drugs such as rapamycin, which may have more pronounced side effects, such as immunosuppression, limiting their long-term use, enalapril has a well-established safety profile(Janes & Fruman, 2009; Saunders, Metcalfe, & Nicholson, 2001). This can facilitate faster clinical translation for anti-aging applications. Moreover, our study revealed that enalapril reduces ROS through the pSmad1/5/9-antioxidant axis, highlighting its potential for antioxidation, a hallmark of aging that is less directly targeted by drugs such as rapamycin or metformin. Additionally, enalapril enhances multi-organ function, particularly in the brain, kidneys, and liver. Its well-established safety profile further supports enalapril as a promising candidate for clinical anti-aging applications, with the potential to complement existing therapies by promoting both vascular health and systemic antioxidative and anti-inflammatory effects.

Aging is a highly complex and multifactorial process(Campisi, 2013; Jazwinski, 1996). It involves intricate interactions among various signaling pathways and crosstalk between tissues and organs, especially during individual aging(Jazwinski, 1996; Munoz-Espin & Serrano, 2014). Notably, enalapril is not uniform across all organs and tissues, as indicated by the differential improvement in aging phenotypes among various tissues. For example, enalapril significantly improved the physiological functions of the brain, muscle and other organs, but the specific pathways and mechanisms by which these effects are mediated might differ among organs. This observation suggests that the tissue-specific effects of enalapril may be mediated by

differential activation of signaling pathways, including those beyond the Smad1/5/9 axis, which are known to play crucial roles in aging. Future studies should focus on delineating these tissue-specific mechanisms to fully understand the scope of the anti-aging effects of enalapril. Moreover, improvements in metabolic function in the liver could have downstream effects on brain function, as metabolic dysregulation is known to exacerbate neurodegenerative diseases. Similarly, enhanced vascular health resulting from the antihypertensive properties of enalapril may contribute to improved brain perfusion, reducing the risk of age-related cognitive decline. Therefore, exploring the systemic effects of enalapril and how improvements in one organ system may benefit others should be a priority for future research. Furthermore, given the established role of enalapril as an antihypertensive drug, assessing its potential side effects when it is repurposed for anti-aging purposes is essential. Identifying strategies to minimize these side effects while optimizing their anti-aging effects is an important area of investigation. In conclusion, our study identified enalapril as a promising candidate for repurposing as an anti-aging drug with antioxidative and promoting effects on cell proliferation. These findings open avenues for the development of targeted therapies aimed at mitigating aging and promoting healthy longevity in clinical settings, providing a foundation for guiding future research in the realm of anti-aging drug interventions.

DATA AVAILABILITY

All related sequencing data have been uploaded to the NCBI Gene Expression Omnibus and are accessible through accession numbers GSE277861 and GSE277862.

ACKNOWLEDGMENTS

We thank Dr. Xuehui Lyu (Peking University) and Shuo Chen (Center for Excellence in Molecular Cell Science, Chinese Academy of Sciences) for suggestions regarding data organization. We thank the National Center for Protein Sciences at Peking University for assisting with the cDNA library and the Core Facilities of Life Sciences, Peking University, for assisting with the confocal microscopy. We are also grateful to the Behavioral Platform of the Animal Center at Peking University for assisting with the behavioral experiments involving the mice.

AUTHOR CONTRIBUTIONS

W.T. oversaw the study and obtained financial support. W.C.L. conducted the main bench experiments. H.C.W. analyzed the data. Z.H.D. and J.N.H. helped prepare the mice samples. R.W., F.J.M. and J.L.B. helped analyze the data. L.J.Z. helped guide the experiment. W.C.L., Y. T. G. and C. Z. prepared the original manuscripts. All the authors read and approved the final version.

FUNDING

This work was supported by the National Key Research and Development Program of China (2021YFA0909300).

COMPETING INTEREST DECLARATION

The authors have no conflicts of interest to declare.

SUPPLEMENTAL INFORMATION

Additional supplementary information includes supplementary figures and tables in the attachment.

REFERENCES

Baker, D. J., Wijshake, T., Tchkonia, T., LeBrasseur, N. K., Childs, B. G., van de Sluis, B., . . . van Deursen, J. M. (2011). Clearance of p16Ink4a-positive senescent cells delays ageing-associated disorders. *Nature, 479*(7372), 232-236. doi:10.1038/nature10600

Bharath, L. P., Agrawal, M., McCambridge, G., Nicholas, D. A., Hasturk, H., Liu, J., . . . Nikolajczyk, B. S. (2020). Metformin Enhances Autophagy and Normalizes Mitochondrial Function to Alleviate Aging-Associated Inflammation. *Cell Metab, 32*(1), 44-55 e46. doi:10.1016/j.cmet.2020.04.015

Campisi, J. (2013). Aging, cellular senescence, and cancer. *Annu Rev Physiol, 75*, 685-705. doi:10.1146/annurev-physiol-030212-183653

Childs, B. G., Gluscevic, M., Baker, D. J., Laberge, R. M., Marquess, D., Dananberg, J., & van Deursen, J. M. (2017). Senescent cells: an emerging target for diseases of ageing. *Nat Rev Drug Discov, 16*(10), 718-735. doi:10.1038/nrd.2017.116

Cohen, A. A., Ferrucci, L., Fülöp, T., Gravel, D., Hao, N., Kriete, A., . . . Varadhan, R. (2022). A complex systems approach to aging biology. *Nature Aging, 2*(7), 580-591. doi:10.1038/s43587-022-00252-6

Coppe, J. P., Patil, C. K., Rodier, F., Sun, Y., Munoz, D. P., Goldstein, J., . . . Campisi, J. (2008). Senescence-associated secretory phenotypes reveal cell-nonautonomous functions of oncogenic RAS and the p53 tumor suppressor. *PLoS Biol, 6*(12), 2853-2868. doi:10.1371/journal.pbio.0060301

Dimri, G. P., Lee, X., Basile, G., Acosta, M., Scott, G., Roskelley, C., . . . et al. (1995). A biomarker that identifies senescent human cells in culture and in aging skin in vivo. *Proc Natl Acad Sci U S A, 92*(20), 9363-9367. doi:10.1073/pnas.92.20.9363

Egan, B. M., Pohl, F., Anderson, X., Williams, S. C., Gregory Adodo, I., Hunt, P., . . . Kornfeld, K. (2024). The ACE inhibitor captopril inhibits ACN-1 to control dauer formation and aging. *Development, 151*(3). doi:10.1242/dev.202146

Fei, M. Y., Wang, Y., Chang, B. H., Xue, K., Dong, F. Y., Huang, D., . . . Wang, L. (2023). The non-cell-autonomous function of ID1 promotes AML progression via ANGPTL7 from the microenvironment. *Blood, 142*(10), 903-917. doi:10.1182/blood.2022019537

Genander, M., Cook, P. J., Ramsköld, D., Keyes, B. E., Mertz, A. F., Sandberg, R., & Fuchs, E. (2014). BMP Signaling and Its pSMAD1/5 Target Genes Differentially Regulate Hair Follicle Stem Cell Lineages. *Cell Stem Cell, 15*(5), 619-633. doi:10.1016/j.stem.2014.09.009

Gu, Z. (2022). Complex heatmap visualization. *Imeta, 1*(3), e43. doi:10.1002/imt2.43

Guglielmi, L., Heliot, C., Kumar, S., Alexandrov, Y., Gori, I., Papaleonidopoulou, F., . . . Hill, C. S. (2021). Smad4 controls signaling robustness and morphogenesis by differentially contributing to the Nodal and BMP pathways. *Nature Communications, 12*(1). doi:ARTN 6374 10.1038/s41467-021-26486-3

Harrison, D. E., Strong, R., Allison, D. B., Ames, B. N., Astle, C. M., Atamna, H., . . . Miller, R. A. (2014). Acarbose, 17-α-estradiol, and nordihydroguaiaretic acid extend mouse lifespan preferentially in males. *Aging Cell, 13*(2), 273-282. doi:10.1111/acel.12170

Harrison, D. E., Strong, R., Sharp, Z. D., Nelson, J. F., Astle, C. M., Flurkey, K., . . . Miller, R. A. (2009). Rapamycin fed late in life extends lifespan in genetically heterogeneous mice. *Nature, 460*(7253), 392-U108. doi:10.1038/nature08221

Hayashi, Y., Hsiao, E. C., Sami, S., Lancero, M., Schlieve, C. R., Nguyen, T., . . . Yamanaka, S. (2016). BMP-SMAD-ID promotes reprogramming to pluripotency by inhibiting p16/INK4A-dependent senescence. *Proc Natl Acad Sci U S A, 113*(46), 13057-13062. doi:10.1073/pnas.1603668113

Janes, M. R., & Fruman, D. A. (2009). Immune Regulation by Rapamycin: Moving Beyond T Cells. *Science Signaling, 2*(67). doi:ARTN pe25 10.1126/scisignal.267pe25

Jazwinski, S. M. (1996). Longevity, genes, and aging. *Science, 273*(5271), 54-59. doi:10.1126/science.273.5271.54

Johnson, A. A., & Stolzing, A. (2019). The role of lipid metabolism in aging, lifespan regulation, and age-related disease. *Aging Cell, 18*(6). doi:ARTN e13048 10.1111/acel.13048

Johnson, S. C., Rabinovitch, P. S., & Kaeberlein, M. (2013). mTOR is a key modulator of ageing and age-related disease. *Nature, 493*(7432), 338-345. doi:10.1038/nature11861

Khosla, S., Farr, J. N., Tchkonia, T., & Kirkland, J. L. (2020). The role of cellular senescence in ageing and endocrine disease. *Nat Rev Endocrinol, 16*(5), 263-275. doi:10.1038/s41574-020-0335-y

Kim, D., Paggi, J. M., Park, C., Bennett, C., & Salzberg, S. L. (2019). Graph-based genome alignment and genotyping with HISAT2 and HISAT-genotype. *Nat Biotechnol, 37*(8), 907-915. doi:10.1038/s41587-019-0201-4

Kirkland, J. L. (2016). Translating the Science of Aging into Therapeutic Interventions. *Cold Spring Harb Perspect Med, 6*(3), a025908. doi:10.1101/cshperspect.a025908

Kumar, S., Dietrich, N., & Kornfeld, K. (2016). Angiotensin Converting Enzyme (ACE) Inhibitor Extends Caenorhabditis elegans Life Span. *PLoS Genet, 12*(2), e1005866. doi:10.1371/journal.pgen.1005866

Langmead, B., & Salzberg, S. L. (2012). Fast gapped-read alignment with Bowtie 2. *Nat Methods, 9*(4), 357-359. doi:10.1038/nmeth.1923

Li, H., Handsaker, B., Wysoker, A., Fennell, T., Ruan, J., Homer, N., . . . Genome Project Data Processing, S. (2009). The Sequence Alignment/Map format and SAMtools. *Bioinformatics, 25*(16), 2078-2079. doi:10.1093/bioinformatics/btp352

Liang, Y. Y., Brunicardi, F. C., & Lin, X. (2009). Smad3 mediates immediate early induction of Id1 by TGF-beta. *Cell Res, 19*(1), 140-148. doi:10.1038/cr.2008.321

Liao, Y., Smyth, G. K., & Shi, W. (2014). featureCounts: an efficient general purpose program for assigning sequence reads to genomic features. *Bioinformatics, 30*(7), 923-930.

doi:10.1093/bioinformatics/btt656

Lihua, Z., Claude, G., & Nathan, L. (2010). ChIPpeakAnno: a Bioconductor package to annotate ChIP-seq and ChIP-chip data. *BMC Bioinformatics, 11*, 237.

Lopez-Otin, C., Blasco, M. A., Partridge, L., Serrano, M., & Kroemer, G. (2023). Hallmarks of aging: An expanding universe. *Cell, 186*(2), 243-278. doi:10.1016/j.cell.2022.11.001

Love, M. I., Huber, W., & Anders, S. (2014). Moderated estimation of fold change and dispersion for RNA-seq data with DESeq2. *Genome Biol, 15*(12), 550. doi:10.1186/s13059-014-0550-8

Lyden, D., Young, A. Z., Zagzag, D., Yan, W., Gerald, W., O'Reilly, R., . . . Benezra, R. (1999). Id1 and Id3 are required for neurogenesis, angiogenesis and vascularization of tumour xenografts. *Nature, 401*(6754), 670-677. doi:10.1038/44334

Lyu, G. L., Guan, Y. T., Zhang, C., Zong, L., Sun, L., Huang, X. K., . . . Tao, W. (2018). TGF-β signaling alters H4K20me3 status via miR-29 and contributes to cellular senescence and cardiac aging (vol 9, 2560, 2018). *Nature Communications, 9*. doi:ARTN 4134 10.1038/s41467-018-06710-3

Miyazono, K., Maeda, S., & Imamura, T. (2005). BMP receptor signaling: Transcriptional targets, regulation of signals, and signaling cross-talk. *Cytokine & Growth Factor Reviews, 16*(3), 251-263. doi:10.1016/j.cytogfr.2005.01.009

Munoz-Espin, D., & Serrano, M. (2014). Cellular senescence: from physiology to pathology. *Nat Rev Mol Cell Biol, 15*(7), 482-496. doi:10.1038/nrm3823

Nadon, N. L., Strong, R., Miller, R. A., Nelson, J., Javors, M., Sharp, Z. D., . . . Harrison, D. E. (2008). Design of aging intervention studies: the NIA interventions testing program. *Age, 30*(4), 187-199. doi:10.1007/s11357-008-9048-1

Orlowski, J. (2017). SMAD5 signaling: more than meets the nuclei. *Cell Res, 27*(9), 1075-1076. doi:10.1038/cr.2017.101

Radulescu, C. I., Cerar, V., Haslehurst, P., Kopanitsa, M., & Barnes, S. J. (2021). The aging mouse brain: cognition, connectivity and calcium. *Cell Calcium, 94*, 102358. doi:10.1016/j.ceca.2021.102358

Rahman, M. S., Akhtar, N., Jamil, H. M., Banik, R. S., & Asaduzzaman, S. M. (2015). TGF-β/BMP signaling and other molecular events: regulation of osteoblastogenesis and bone formation. *Bone Research, 3*. doi:ARTN 15005 10.1038/boneres.2015.5

Ramachandran, A., Vizán, P., Das, D., Chakravarty, P., Vogt, J., Rogers, K. W., . . . Hill, C. S. (2018). TGF-β uses a novel mode of receptor activation to phosphorylate SMAD1/5 and induce epithelial-to-mesenchymal transition. *Elife, 7*. doi:ARTN e31756 10.7554/eLife.31756

Ramirez, F., Dundar, F., Diehl, S., Gruning, B. A., & Manke, T. (2014). deepTools: a flexible platform for exploring deep-sequencing data. *Nucleic Acids Res, 42*(Web Server issue), W187-191. doi:10.1093/nar/gku365

Saunders, R. N., Metcalfe, M. S., & Nicholson, M. L. (2001). Rapamycin in transplantation: A

review of the evidence. *Kidney International, 59*(1), 3-16. doi:DOI 10.1046/j.1523-1755.2001.00460.x

Schmieder, R. E., Hilgers, K. F., Schlaich, M. P., & Schmidt, B. M. W. (2007). Renin-angiotensin system and cardiovascular risk. *Lancet, 369*(9568), 1208-1219. doi:10.1016/S0140-6736(07)60242-6

Senft, A. D., Bikoff, E. K., Robertson, E. J., & Costello, I. (2019). Genetic dissection of Nodal and Bmp signalling requirements during primordial germ cell development in mouse. *Nature Communications, 10*. doi:ARTN 1089 10.1038/s41467-019-09052-w

Shah, P. P., Donahue, G., Otte, G. L., Capell, B. C., Nelson, D. M., Cao, K., . . . Berger, S. L. (2013). Lamin B1 depletion in senescent cells triggers large-scale changes in gene expression and the chromatin landscape. *Genes Dev, 27*(16), 1787-1799. doi:10.1101/gad.223834.113

Strong, R., Miller, R. A., Antebi, A., Astle, C. M., Bogue, M., Denzel, M. S., . . . Harrison, D. E. (2016). Longer lifespan in male mice treated with a weakly estrogenic agonist, an antioxidant, an -glucosidase inhibitor or a Nrf2-inducer. *Aging Cell, 15*(5), 872-884. doi:10.1111/acel.12496

Strong, R., Miller, R. A., Cheng, C. J., Nelson, J. F., Gelfond, J., Allani, S. K., . . . Harrison, D. E. (2022). Lifespan benefits for the combination of rapamycin plus acarbose and for captopril in genetically heterogeneous mice. *Aging Cell, 21*(12). doi:10.1111/acel.13724

Sun, Y., Yan, K., Wang, Y., Xu, C., Wang, D., Zhou, W., . . . Xi, Q. R. (2022). Context-dependent tumor-suppressive BMP signaling in diffuse intrinsic pontine glioma regulates stemness through epigenetic regulation of CXXC5. *Nature Cancer, 3*(9), 1105-+. doi:10.1038/s43018-022-00408-8

Urist, M. R. (1965). Bone - Formation by Autoinduction. *Science, 150*(3698), 893-+. doi:DOI 10.1126/science.150.3698.893

Wu, T., Hu, E., Xu, S., Chen, M., Guo, P., Dai, Z., . . . Yu, G. (2021). clusterProfiler 4.0: A universal enrichment tool for interpreting omics data. *Innovation (Camb), 2*(3), 100141. doi:10.1016/j.xinn.2021.100141

Xu, M., Pirtskhalava, T., Farr, J. N., Weigand, B. M., Palmer, A. K., Weivoda, M. M., . . . Kirkland, J. L. (2018). Senolytics improve physical function and increase lifespan in old age. *Nat Med, 24*(8), 1246-1256. doi:10.1038/s41591-018-0092-9

Yamamoto, K., & Rakugi, H. (2021). Angiotensin receptor-neprilysin inhibitors: Comprehensive review and implications in hypertension treatment. *Hypertension Research, 44*(10), 1239-1250. doi:10.1038/s41440-021-00706-1

Ying, Q. L., Nichols, J., Chambers, I., & Smith, A. (2003). BMP induction of Id proteins suppresses differentiation and sustains embryonic stem cell self-renewal in collaboration with STAT3. *Cell, 115*(3), 281-292. doi:Doi 10.1016/S0092-8674(03)00847-X

Yousefzadeh, M. J., Zhu, Y., McGowan, S. J., Angelini, L., Fuhrmann-Stroissnigg, H., Xu, M., . . . Niedernhofer, L. J. (2018). Fisetin is a senotherapeutic that extends health and lifespan. *Ebiomedicine, 36*, 18-28. doi:10.1016/j.ebiom.2018.09.015

Zhang, Y., Liu, T., Meyer, C. A., Eeckhoute, J., Johnson, D. S., Bernstein, B. E., . . . Liu, X. S. (2008). Model-based analysis of ChIP-Seq (MACS). *Genome Biol, 9*(9), R137. doi:10.1186/gb-2008-9-9-r137

Zhou, Y., Zhou, B., Pache, L., Chang, M., Khodabakhshi, A. H., Tanaseichuk, O., . . . Chanda, S. K. (2019). Metascape provides a biologist-oriented resource for the analysis of systems-level datasets. *Nat Commun, 10*(1), 1523. doi:10.1038/s41467-019-09234-6

Zhu, Y., Tchkonia, T., Fuhrmann-Stroissnigg, H., Dai, H. M. M., Ling, Y. Y. Y., Stout, M. B., . . . Kirkland, J. L. (2016). Identification of a novel senolytic agent, navitoclax, targeting the Bcl-2 family of anti-apoptotic factors. *Aging Cell, 15*(3), 428-435. doi:10.1111/acel.12445

Zhu, Y., Tchkonia, T., Pirtskhalava, T., Gower, A. C., Ding, H. S., Giorgadze, N., . . . Kirkland, J. L. (2015). The Achilles' heel of senescent cells: from transcriptome to senolytic drugs. *Aging Cell, 14*(4), 644-658. doi:10.1111/acel.12344

FIGURE AND FIGURE LEGENDS

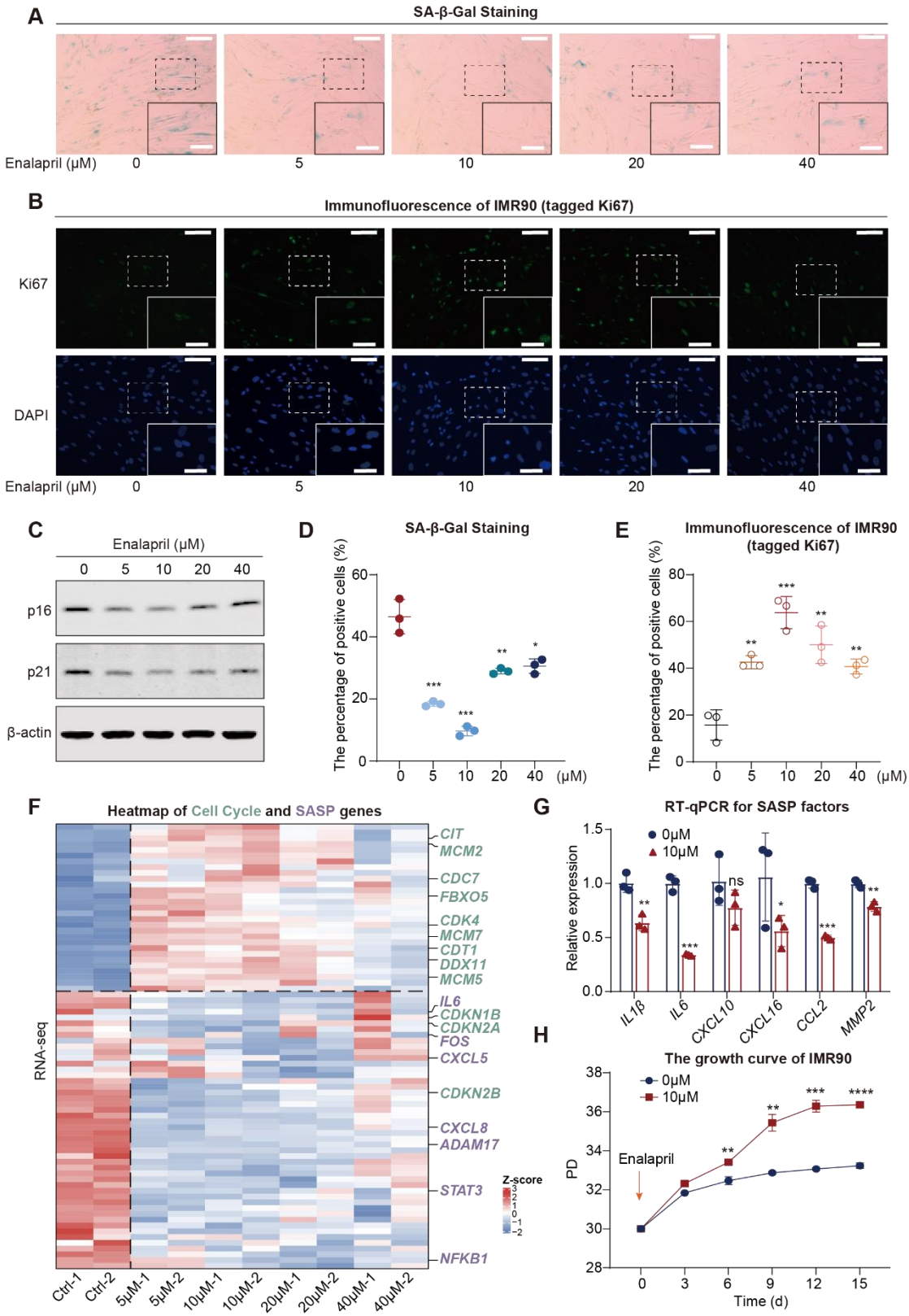

Figure 1 Enalapril alleviates cellular senescence. (**A, D**) SA-β-Gal staining (**A**) and statistical analysis of SA-β-Gal ratios (**D**) in IMR90 cells after enalapril treatment. Scale

794 bars, 200 μm. Enlarged scale bars, 100 μm. (**B, E**) Ki67 immunofluorescence
795 experiment (**B**) and statistical analysis of Ki67 intensity (**E**) after enalapril treatment.
796 Scale bars, 80 μm. Enlarged scale bars, 40 μm. (**C**) Western blot analysis showing the
797 protein levels of p16 and p21 in IMR90 cells after enalapril treatment. (**F**) Heatmap
798 showing cell cycle-related gene (green) upregulation and SASP gene (purple)
799 downregulation after enalapril treatment. (**G**) RNA expression of SASP factors in
800 IMR90 cells after enalapril treatment, with blue bars representing the control group and
801 red bars representing the enalapril-treated group. (**H**) Growth curves of IMR90 cells
802 after enalapril treatment. The x-axis represents the passage time, while the y-axis
803 represents population doubling (PD). A two-tailed t test was employed; ns indicates no
804 significant difference, *$p < 0.05$, **$p < 0.01$, ***$p < 0.001$, ****$p < 0.0001$.

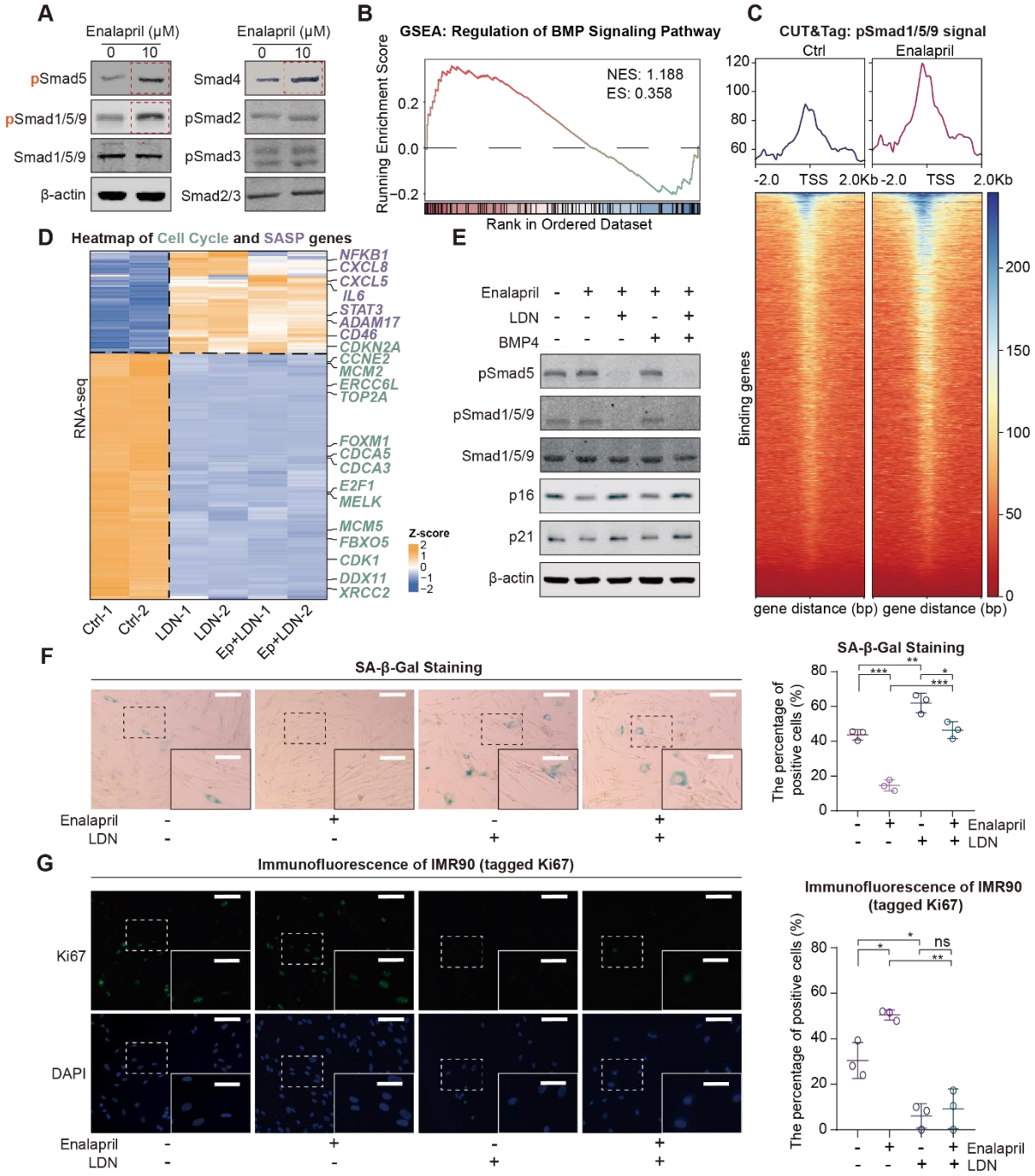

Figure 2 Phosphorylated Smad1/5/9 mediate the anti-senescence effect of enalapril. (**A**) Western blot results for the detection of pSmad5, pSmad1/5/9 and other proteins after enalapril treatment. (**B**) GSEA showing the enrichment of the BMP signaling pathway after enalapril treatment. NES, normalized enrichment score. ES, enrichment score. (**C**) Profile of pSmad1/5/9 enrichment at the TSS regions in the control group (Ctrl) and the enalapril-treated group (Enalapril). (**D**) Heatmap of cell cycle (green) and SASP-related genes (purple) in the control group (Ctrl), BMP receptor inhibitor-treated group (LDN193189, LDN), and enalapril and BMP receptor inhibitor-cotreated group

(EP+LDN). (**E**) Western blot analysis showing the protein levels of pSmad1/5/9, p16, and p21 in response to different combinations of enalapril, a BMP receptor inhibitor (LDN193189, LDN), and BMP4. (**F**) SA-β-Gal staining (left) and corresponding ratio statistical chart (right) of IMR90 cells treated with different combinations of enalapril, a BMP receptor inhibitor (LDN193189, LDN), and BMP4. Scale bars, 200 μm. Enlarged scale bars, 100 μm. (**G**) Ki67 immunofluorescence experiment (left) and intensity statistical chart (right) of IMR90 cells treated with different combinations of enalapril, a BMP receptor inhibitor (LDN193189, LDN), and BMP4. Scale bars, 80 μm. Enlarged scale bars, 40 μm. A two-tailed t test was employed; ns indicates no significant difference, $^{*}p < 0.05$, $^{**}p < 0.01$, $^{***}p < 0.001$.

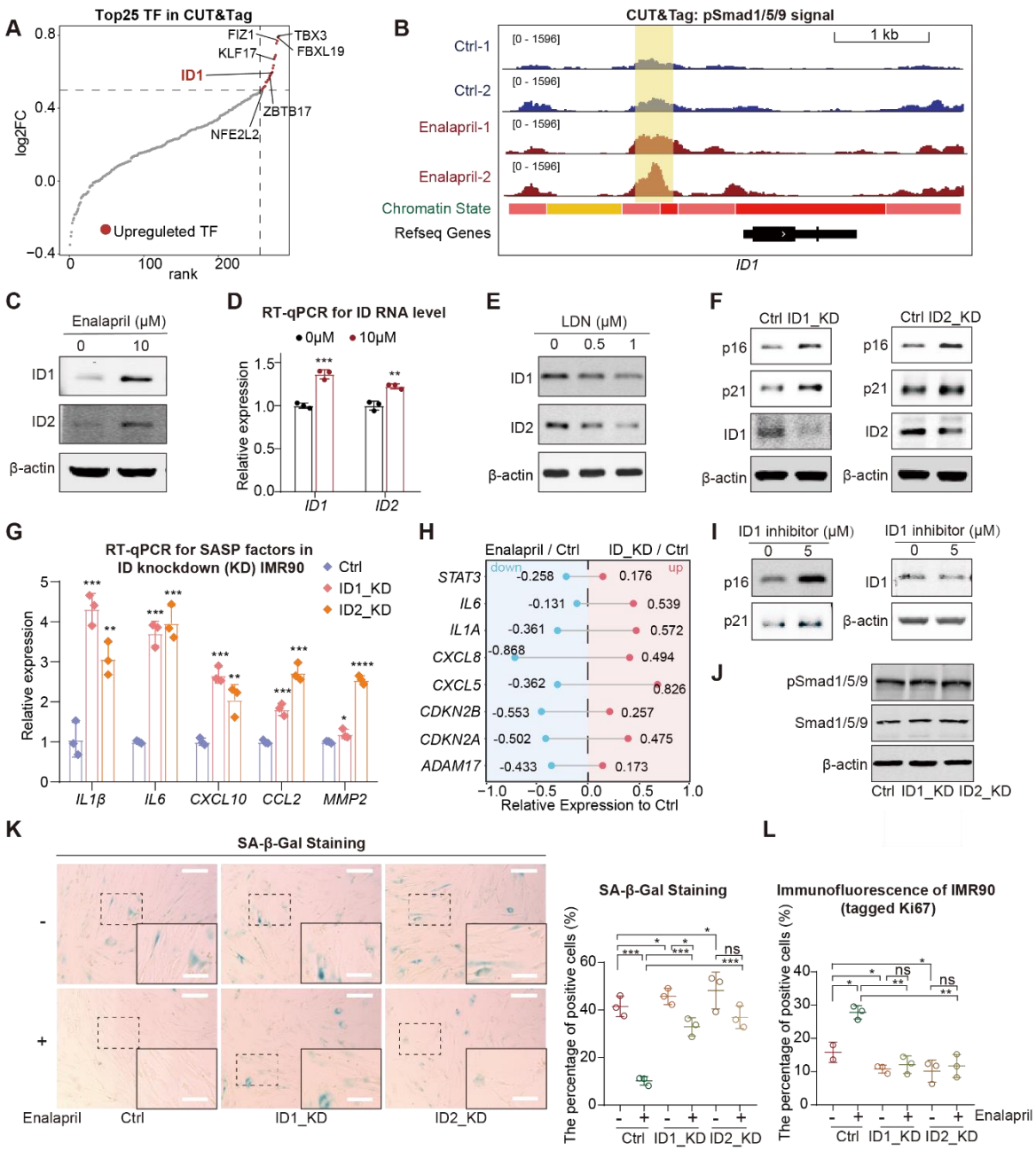

Figure 3 pSmad1/5/9 regulate ID-induced inhibition of p16, p21 and SASP. (**A**) Changes in the peaks of all transcription factors identified by CUT&Tag following enalapril treatment, with red dots indicating transcription factors with increased peak intensity (Upregulated TFs). (**B**) Integrative Genomics Viewer (IGV) showing pSmad1/5/9 signals near the *ID1* region between the control group (Ctrl) and the enalapril treatment group (Enalapril). The vertical yellow boxes indicate regions with increased signal intensity. (**C**) Western blot analysis showing the changes in the protein levels of ID1 and ID2 following enalapril treatment. (**D**) Changes in the RNA levels of ID1 and ID2 following enalapril treatment. (**E**) Western blot analysis showing the protein levels of ID1 and ID2 following treatment with a BMP receptor inhibitor

835 (LDN193189, LDN). (**F, I**) Western blot showing the changes in the protein levels of
836 p16 and p21 following the knockdown of *ID1* or *ID2* (**F**) or the inhibition of ID1 (**I**).
837 (**G**) RNA expression of SASP factors after *ID* knockdown, with pink representing *ID1*
838 knockdown and orange representing *ID2* knockdown. (**H**) Normalized average RNA
839 expression levels of selected SASP factors and cell cycle arrest factors after enalapril
840 treatment and *ID* knockdown. Positive values indicate upregulation, while negative
841 values indicate downregulation. The values represent the expression levels relative to
842 those of the Ctrl. (**J**) Western blot analysis showing pSmad1/5/9 levels following *ID1*
843 and *ID2* knockdown. (**K**) SA-β-Gal staining (left) and SA-β-Gal ratio quantification
844 (right) in the control group (Ctrl) and *ID*-knockdown groups (ID1_KD, ID2_KD) with
845 or without enalapril treatment. Scale bars, 200 μm. Enlarged scale bars, 100 μm. (L)
846 Ki67 immunofluorescence intensity in the control group (Ctrl) and *ID* knockdown
847 groups (ID1_KD, ID2_KD), with or without enalapril treatment. A two-tailed t test was
848 employed; ns indicates no significant difference, *$p < 0.05$, **$p < 0.01$, ***$p < 0.001$.

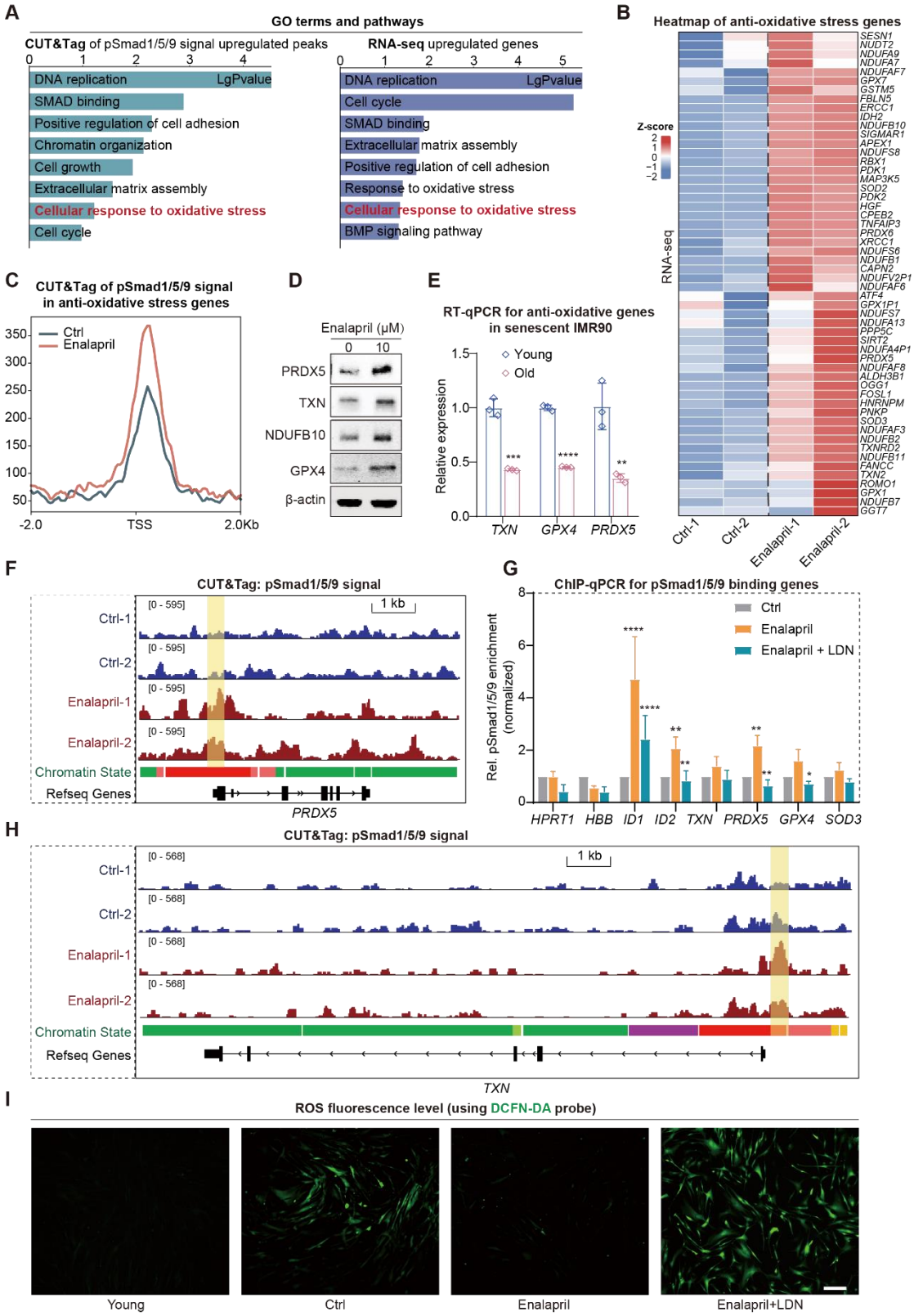

Figure 4 pSmad1/5/9 increase the expression of antioxidative genes. (**A**) Bar plot showing the enriched GO terms and pathways associated with the CUT&Tag-upregulated peaks (left) and the upregulated RNA-seq genes (right) following enalapril treatment. (**B**) Heatmap showing the changes in the RNA expression of antioxidative

genes. (**C**) Profile plot showing the increase in the pSmad1/5/9 binding signal of antioxidative genes in the TSS region following enalapril treatment. (**D**) Western blot analysis showing the protein levels of representative antioxidative genes after enalapril treatment. (**E**) Relative RNA levels of *TXN*, *GPX4*, and *PRDX5* during cellular senescence. The blue bars represent young cells, and the red bars represent senescent cells. (**F, H**) Integrative Genomics Viewer (IGV) showing pSmad1/5/9 signals near the *PRDX5* (**F**) and *TXN* (**H**) regions between the control group (Ctrl) and the enalapril treatment group (Enalapril). The vertical yellow boxes indicate regions with increased signal intensity. (**G**) ChIP-qPCR results showing pSmad1/5/9 levels at many peaks following enalapril or combination treatment with enalapril and LDN193189. The y-axis represents the normalized pSmad1/5/9 signals relative to 10% input. pSmad1/5/9 enrichment for *HPRT1* and *HBB* served as a negative control, and pSmad1/5/9 enrichment for *ID1* and *ID2* served as positive controls, as previously described. A two-tailed t test was employed, $*p < 0.05$, $**p < 0.01$, $***p < 0.001$, $****p < 0.0001$. (**I**) Detection of ROS fluorescence levels via the DCFH-DA probe in young cells, senescent cells (Ctrl), cells treated with enalapril, and cells treated with a combination of enalapril and LDN193189. Scale bars, 200 μm.

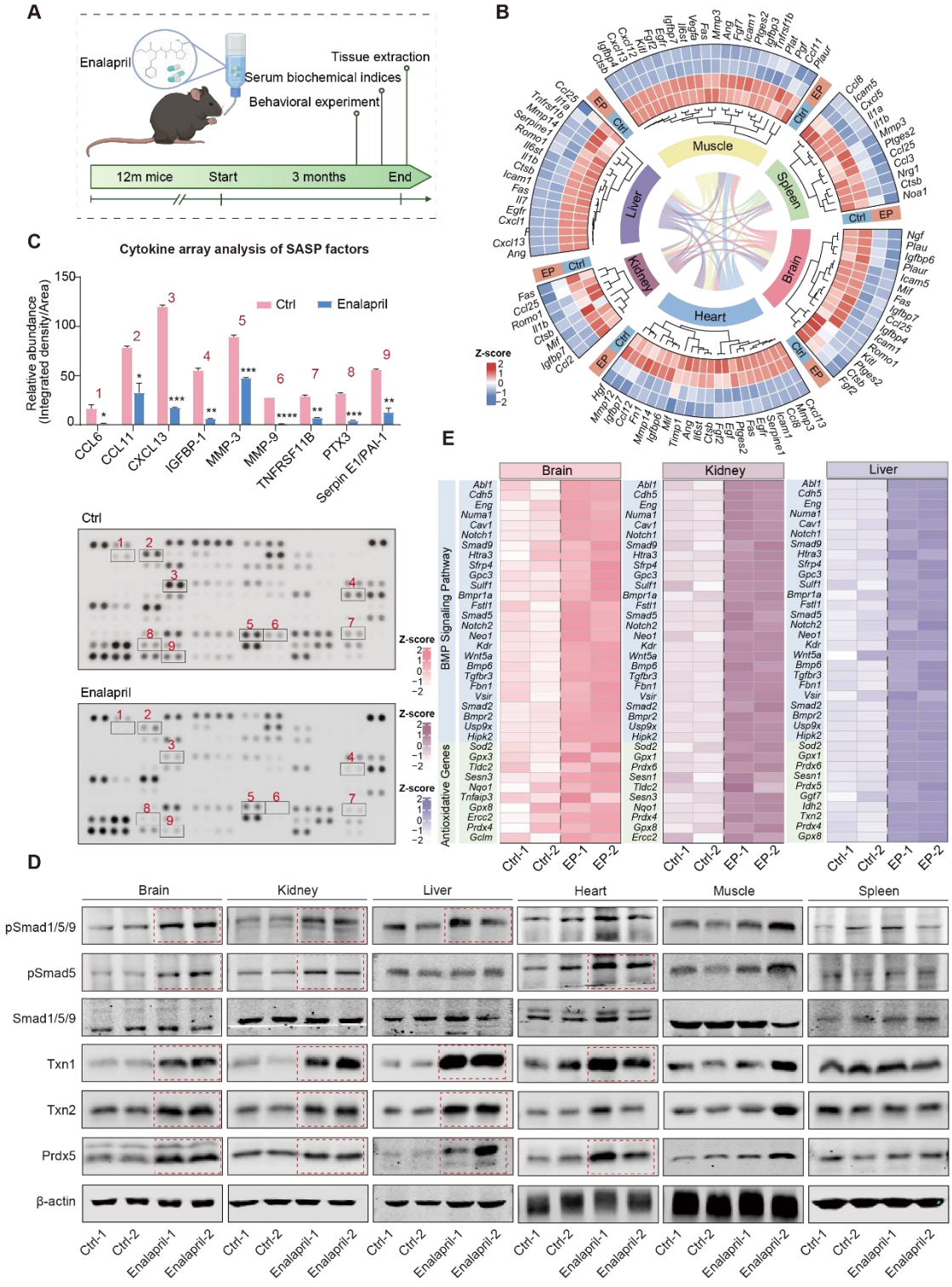

Figure 5 Enalapril exerts its anti-aging effects on mouse organs via pSmad1/5/9-antioxidative genes. (**A**) A schematic workflow of the mouse feeding and experimental procedures. Created in BioRender. Li, D. (2024) BioRender.com/u88h339 (**B**) Heatmap of RNA levels of SASP factors in various organs following enalapril treatment (EP). (**C**) Cytokine array analysis of secreted proteins (below) and relative quantitation

877 (above) of SASP factors in control serum (Ctrl) and enalapril-treated serum (Enalapril).
878 (**D**) Western blot analysis showing the protein levels of pSmad1/5/9 and antioxidative
879 genes in various organs following enalapril treatment. (**E**) Heatmap of the RNA levels
880 of BMP signaling pathway-related genes and antioxidative genes in the brain, kidney,
881 and liver following enalapril (EP) treatment.

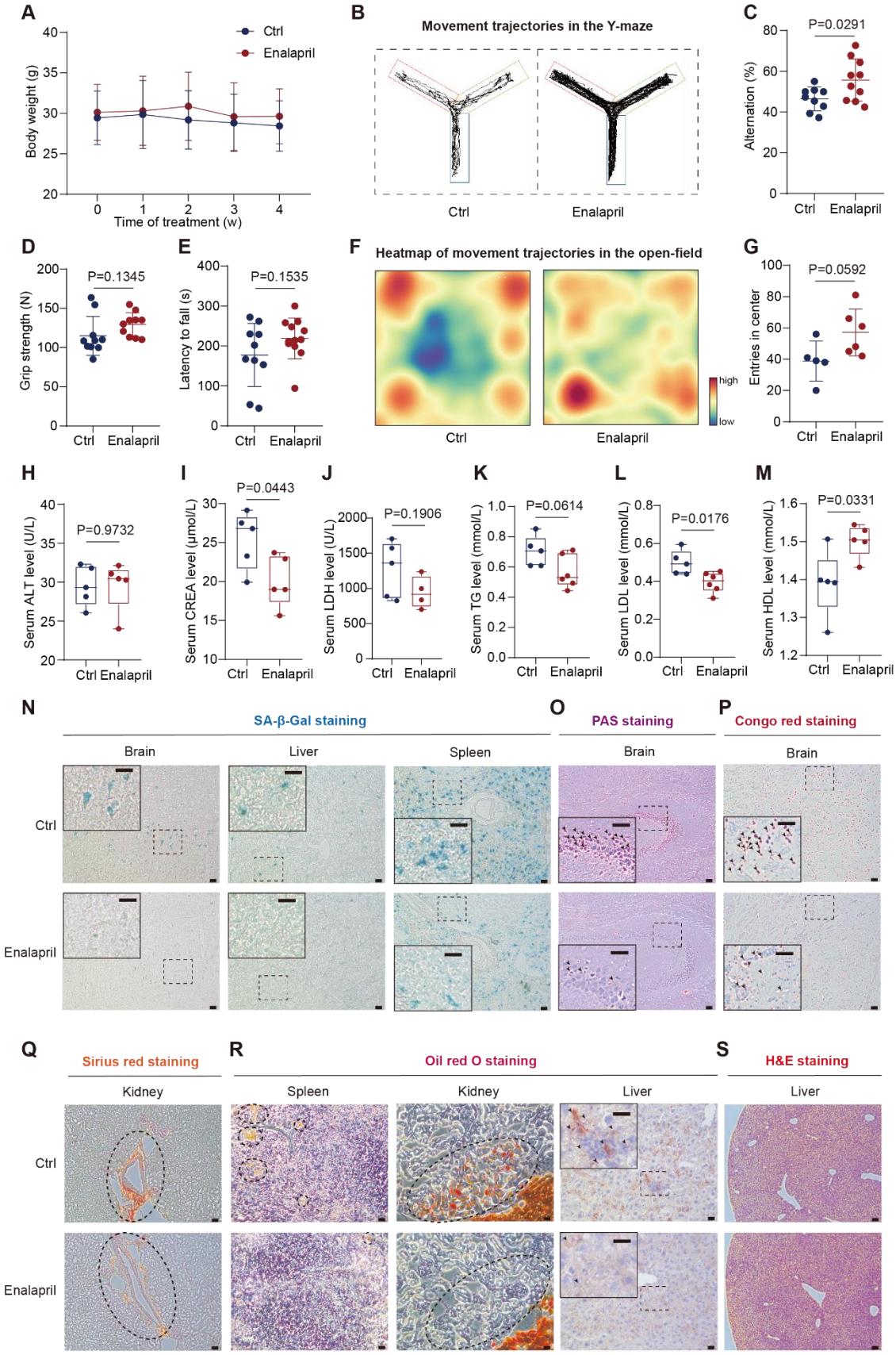

Figure 6 Enalapril mitigates age-related degenerative changes in aged mice. (**A**) Changes in the body weights of the mice after enalapril feeding. (**B, C**) Movement

trajectory (**B**) and spontaneous alternation rate (**C**) in the Y-maze of the mice after enalapril treatment. (**D, E**) Changes in the grip strength (**D**) and rotarod fall time (**E**) of the mice after enalapril treatment. (**F, G**) Heatmap of movement trajectories (**F**) and the number of entries into the central area (**G**) in the open-field test after enalapril treatment. (**H–M**) Alterations in the serum levels of aspartate transaminase (AST) (**H**), creatinine (CREA) (**I**), lactate dehydrogenase (LDH) (**J**), triglycerides (TGs) (**K**), low-density lipoprotein cholesterol (LDL) (**L**), and high-density lipoprotein cholesterol (HDL) (**M**) after enalapril treatment in mice. (**N**) SA-β-Gal staining of the brain, liver, and spleen after enalapril treatment. Scale bars, 20 μm. (**O, P**) Periodic Acid-Schiff (PAS) staining (**O**) and Congo red staining (**P**) of the brain after enalapril treatment. Scale bars, 50 μm. (**Q**) Sirius red staining of the kidney after enalapril treatment. Scale bars, 50 μm. (**R**) Oil Red O staining of the spleen, kidney and liver after enalapril treatment. Scale bars, 20 μm. (**S**) Hematoxylin and eosin (H&E) staining of the liver after enalapril treatment. Scale bars, 50 μm.

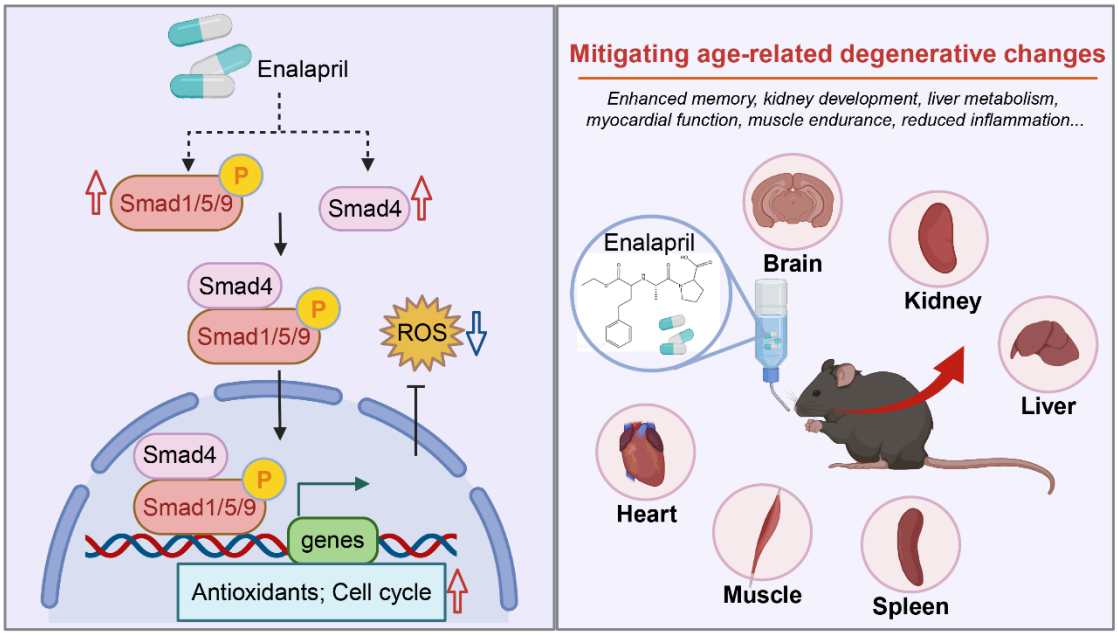

Figure 7 Summary schematic. It showing pSmad1/5/9-mediated combating cellular senescence of enalapril, and improvement of organ function in mice. Specifically, enalapril increases the level of pSmad1/5/9 and Smad4, promoting the expression of downstream genes, such as antioxidative and cell cycle related genes, thereby promoting cell proliferation and reducing ROS. Moreover, enalapril mitigates age-related degenerative changes, including enhanced memory, improved kidney function, increased liver metabolism and other organ functions. Created in BioRender. Li, D. (2024) BioRender.com/u88h339.

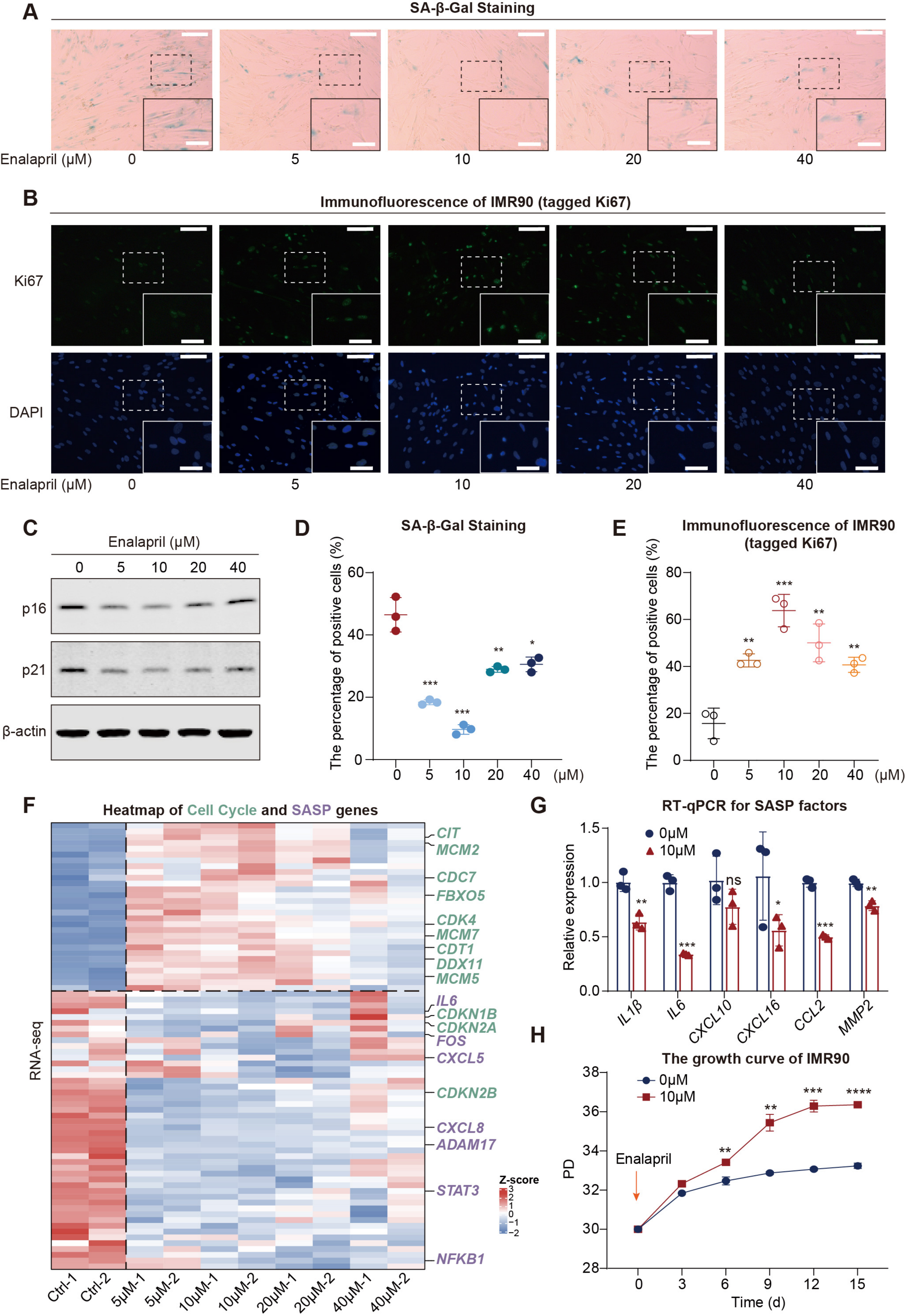
A
SA-β-Gal Staining
Enalapril (μM)
0
5
10
20
40
B
Immunofluorescence of IMR90 (tagged Ki67)
Ki67
DAPI
Enalapril (μM)
0
5
10
20
40
C
Enalapril (μM)
0
5
10
20
40
p16
p21
β-actin
D
SA-β-Gal Staining
The percentage of positive cells (%)
60
40
20
0
0
5
10
20
40
(μM)
***
***
**
*
E
Immunofluorescence of IMR90 (tagged Ki67)
The percentage of positive cells (%)
80
60
40
20
0
0
5
10
20
40
(μM)
**
***
**
**
F
Heatmap of Cell Cycle and SASP genes
RNA-seq
CIT
MCM2
CDC7
FBXO5
CDK4
MCM7
CDT1
DDX11
MCM5
IL6
CDKN1B
CDKN2A
FOS
CXCL5
CDKN2B
CXCL8
ADAM17
STAT3
NFKB1
Z-score
3
2
1
0
−1
−2
Ctrl-1
Ctrl-2
5μM-1
5μM-2
10μM-1
10μM-2
20μM-1
20μM-2
40μM-1
40μM-2
G
RT-qPCR for SASP factors
Relative expression
1.5
1.0
0.5
0.0
0μM
10μM
**
***
ns
*
***
**
IL1β
IL6
CXCL10
CXCL16
CCL2
MMP2
H
The growth curve of IMR90
PD
38
36
34
32
30
28
0μM
10μM
Enalapril
**
**
***
****
0
3
6
9
12
15
Time (d)

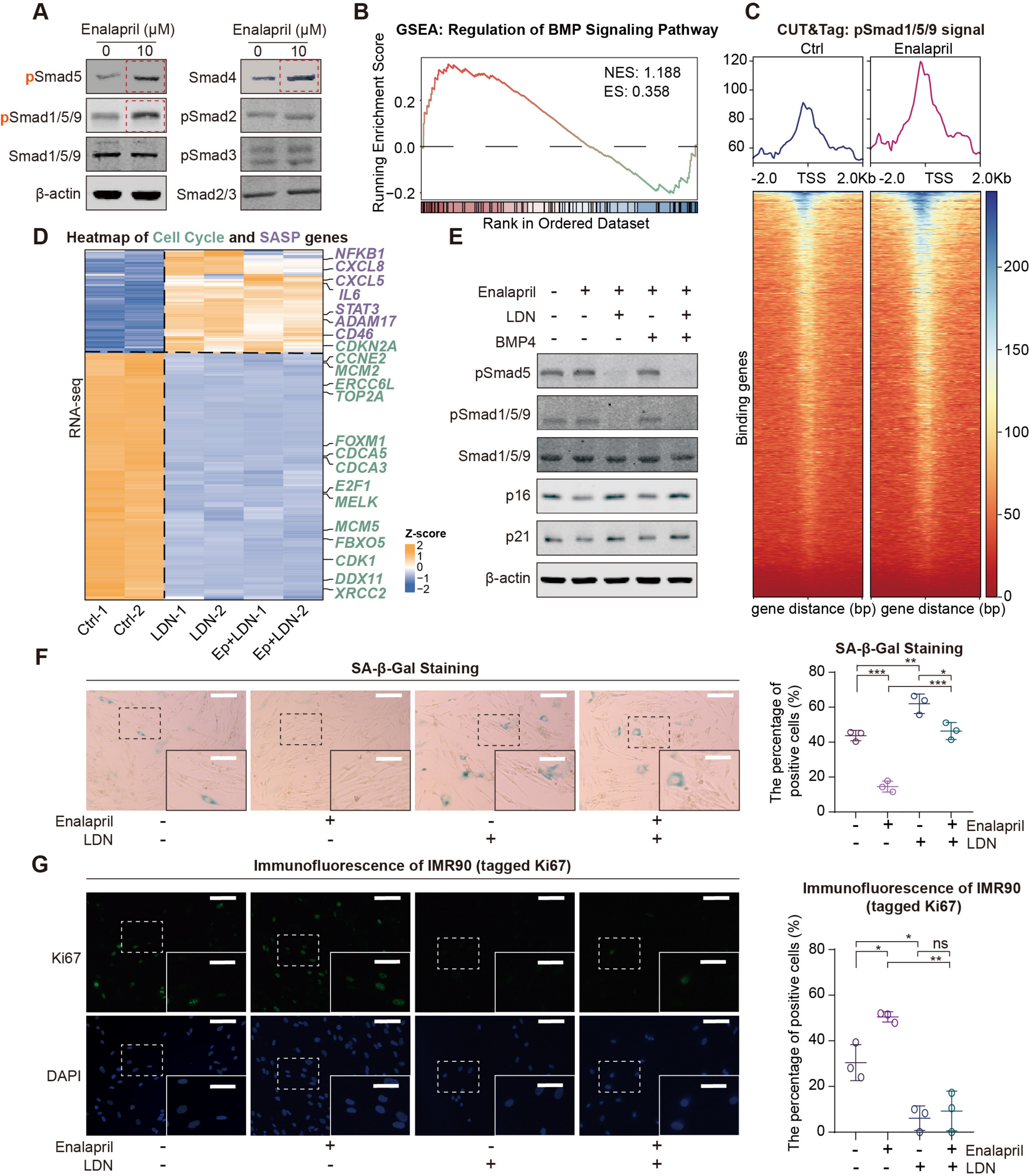
A
Enalapril (μM)
0
10
pSmad5
pSmad1/5/9
Smad1/5/9
β-actin
Smad4
pSmad2
pSmad3
Smad2/3
B
GSEA: Regulation of BMP Signaling Pathway
NES: 1.188
ES: 0.358
Running Enrichment Score
Rank in Ordered Dataset
C
CUT&Tag: pSmad1/5/9 signal
Ctrl
Enalapril
-2.0
TSS
2.0Kb
Binding genes
gene distance (bp)
D
Heatmap of Cell Cycle and SASP genes
RNA-seq
NFKB1
CXCL8
CXCL5
IL6
STAT3
ADAM17
CD46
CDKN2A
CCNE2
MCM2
ERCC6L
TOP2A
FOXM1
CDCA5
CDCA3
E2F1
MELK
MCM5
FBXO5
CDK1
DDX11
XRCC2
Z-score
Ctrl-1
Ctrl-2
LDN-1
LDN-2
Ep+LDN-1
Ep+LDN-2
E
Enalapril
LDN
BMP4
pSmad5
pSmad1/5/9
Smad1/5/9
p16
p21
β-actin
F
SA-β-Gal Staining
Enalapril
LDN
The percentage of positive cells (%)
G
Immunofluorescence of IMR90 (tagged Ki67)
Ki67
DAPI
Enalapril
LDN
The percentage of positive cells (%)

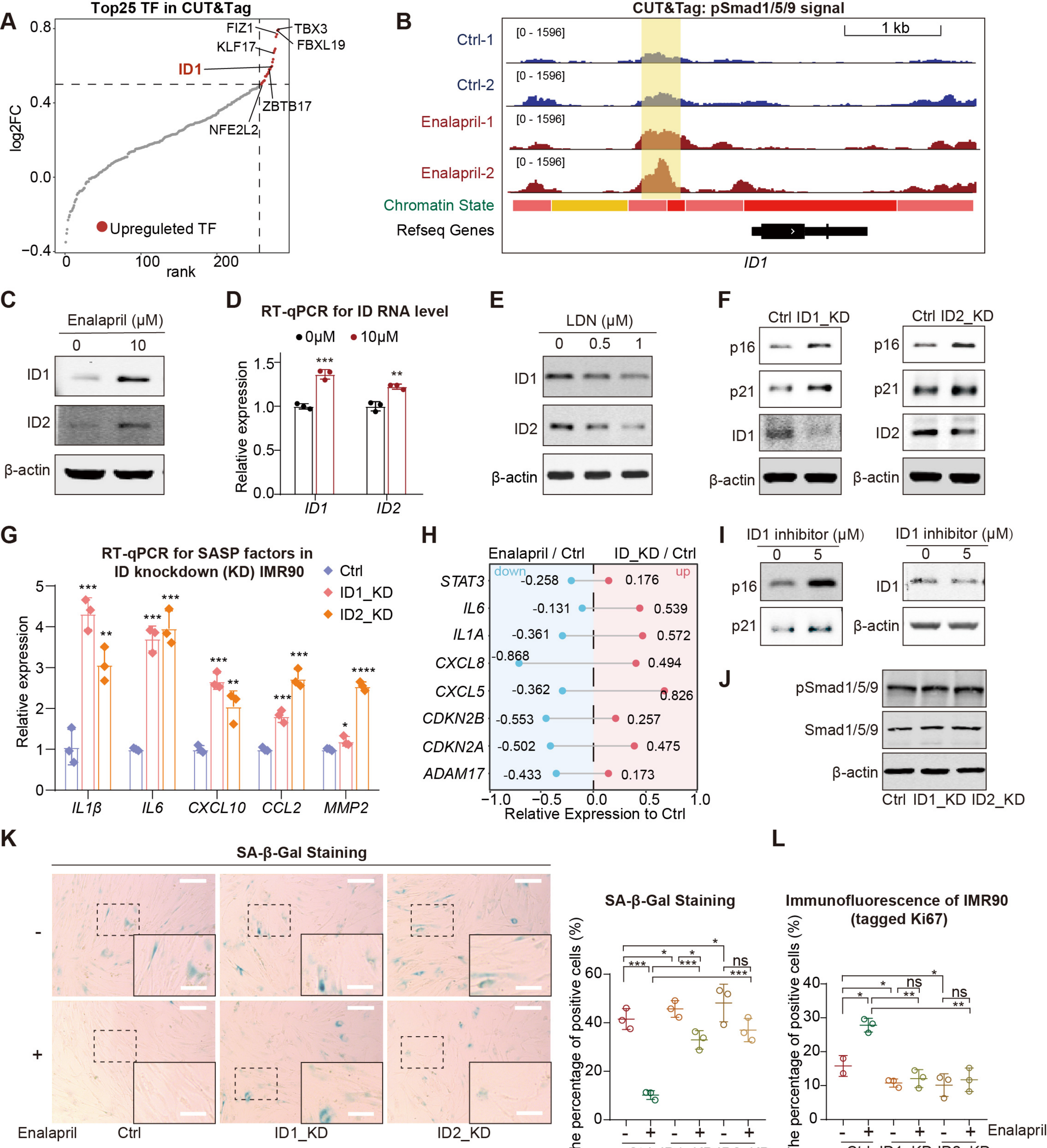
A
Top25 TF in CUT&Tag
FIZ1
TBX3
FBXL19
KLF17
ID1
ZBTB17
NFE2L2
Upreguleted TF
log2FC
rank
B
CUT&Tag: pSmad1/5/9 signal
Ctrl-1
Ctrl-2
Enalapril-1
Enalapril-2
Chromatin State
Refseq Genes
[0 - 1596]
1 kb
ID1
C
Enalapril (μM)
0
10
ID1
ID2
β-actin
D
RT-qPCR for ID RNA level
0μM
10μM
Relative expression
ID1
ID2
E
LDN (μM)
0
0.5
1
ID1
ID2
β-actin
F
Ctrl ID1_KD
Ctrl ID2_KD
p16
p21
ID1
ID2
β-actin
G
RT-qPCR for SASP factors in ID knockdown (KD) IMR90
Ctrl
ID1_KD
ID2_KD
Relative expression
IL1β
IL6
CXCL10
CCL2
MMP2
H
Enalapril / Ctrl
ID_KD / Ctrl
down
up
STAT3 -0.258 0.176
IL6 -0.131 0.539
IL1A -0.361 0.572
CXCL8 -0.868 0.494
CXCL5 -0.362 0.826
CDKN2B -0.553 0.257
CDKN2A -0.502 0.475
ADAM17 -0.433 0.173
Relative Expression to Ctrl
I
ID1 inhibitor (μM)
0
5
p16
p21
ID1
β-actin
J
pSmad1/5/9
Smad1/5/9
β-actin
Ctrl
ID1_KD
ID2_KD
K
SA-β-Gal Staining
Enalapril
Ctrl
ID1_KD
ID2_KD
L
SA-β-Gal Staining
Immunofluorescence of IMR90 (tagged Ki67)
The percentage of positive cells (%)
Enalapril

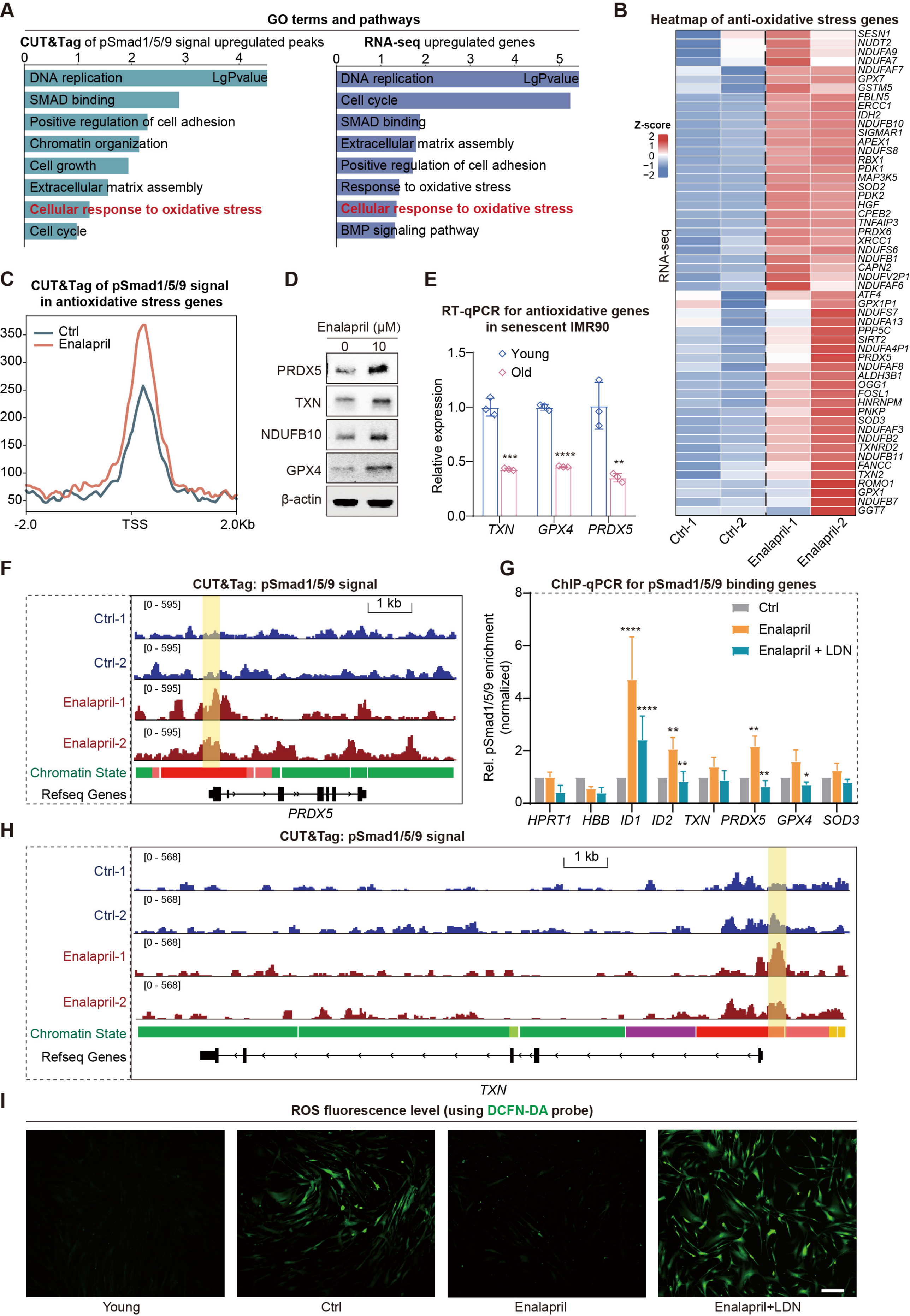
A
GO terms and pathways
CUT&Tag of pSmad1/5/9 signal upregulated peaks
DNA replication
SMAD binding
Positive regulation of cell adhesion
Chromatin organization
Cell growth
Extracellular matrix assembly
Cellular response to oxidative stress
Cell cycle
LgPvalue
RNA-seq upregulated genes
DNA replication
Cell cycle
SMAD binding
Extracellular matrix assembly
Positive regulation of cell adhesion
Response to oxidative stress
Cellular response to oxidative stress
BMP signaling pathway
B
Heatmap of anti-oxidative stress genes
Z-score
RNA-seq
Ctrl-1
Ctrl-2
Enalapril-1
Enalapril-2
C
CUT&Tag of pSmad1/5/9 signal in antioxidative stress genes
Ctrl
Enalapril
-2.0
TSS
2.0Kb
D
Enalapril (μM)
0
10
PRDX5
TXN
NDUFB10
GPX4
β-actin
E
RT-qPCR for antioxidative genes in senescent IMR90
Young
Old
Relative expression
TXN
GPX4
PRDX5
F
CUT&Tag: pSmad1/5/9 signal
Ctrl-1
Ctrl-2
Enalapril-1
Enalapril-2
Chromatin State
Refseq Genes
1 kb
PRDX5
G
ChIP-qPCR for pSmad1/5/9 binding genes
Ctrl
Enalapril
Enalapril + LDN
Rel. pSmad1/5/9 enrichment (normalized)
HPRT1
HBB
ID1
ID2
TXN
PRDX5
GPX4
SOD3
H
CUT&Tag: pSmad1/5/9 signal
Ctrl-1
Ctrl-2
Enalapril-1
Enalapril-2
Chromatin State
Refseq Genes
1 kb
TXN
I
ROS fluorescence level (using DCFN-DA probe)
Young
Ctrl
Enalapril
Enalapril+LDN

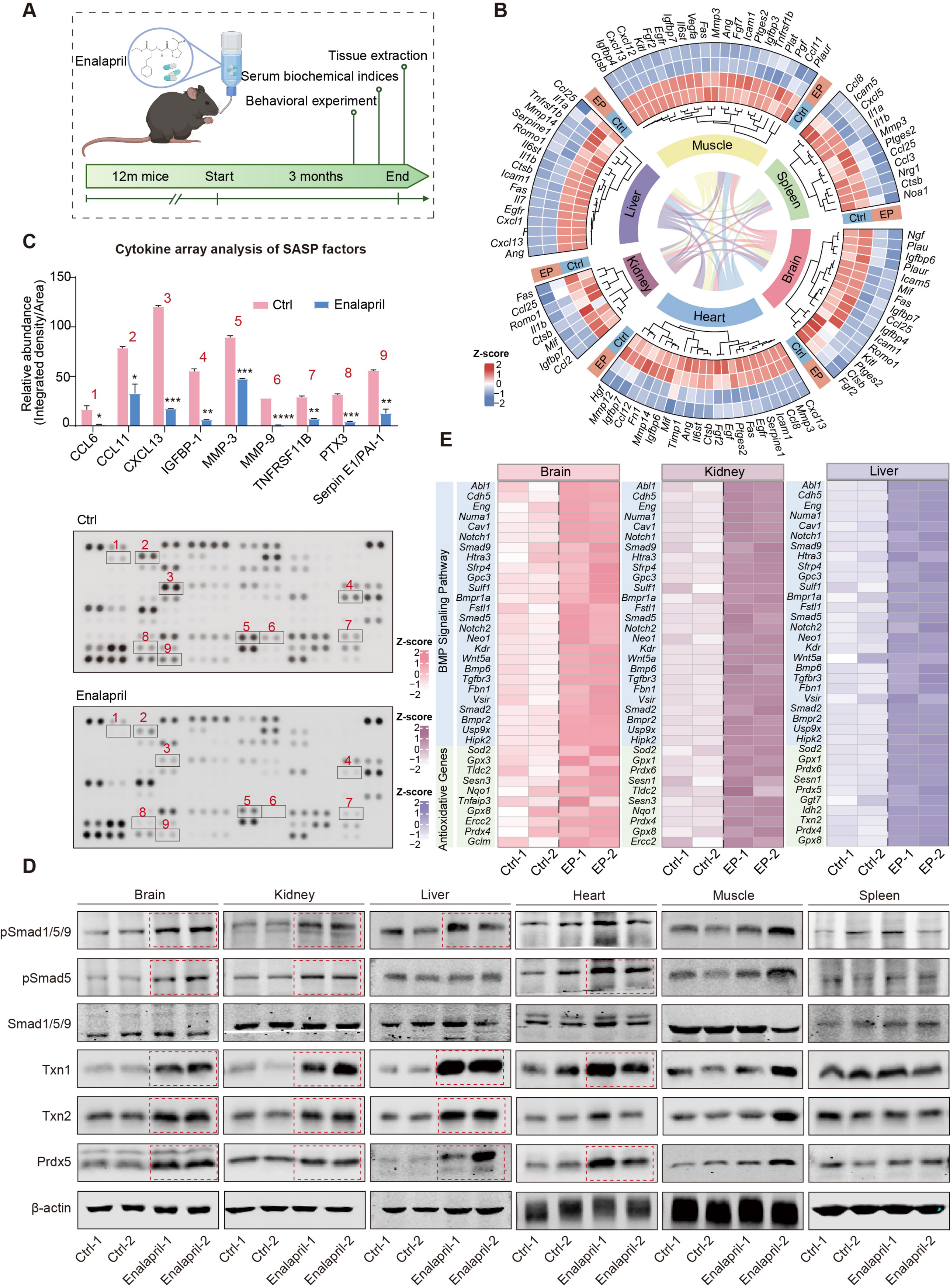
A
Enalapril
Tissue extraction
Serum biochemical indices
Behavioral experiment
12m mice
Start
3 months
End
B
Muscle
Spleen
Brain
Heart
Kidney
Liver
EP
Ctrl
Z-score
C
Cytokine array analysis of SASP factors
Relative abundance (Integrated density/Area)
Ctrl
Enalapril
CCL6
CCL11
CXCL13
IGFBP-1
MMP-3
MMP-9
TNFRSF11B
PTX3
Serpin E1/PAI-1
Ctrl
Enalapril
D
Brain
Kidney
Liver
Heart
Muscle
Spleen
pSmad1/5/9
pSmad5
Smad1/5/9
Txn1
Txn2
Prdx5
β-actin
Ctrl-1
Ctrl-2
Enalapril-1
Enalapril-2
E
BMP Signaling Pathway
Antioxidative Genes
Abl1
Cdh5
Eng
Numa1
Cav1
Notch1
Smad9
Htra3
Sfrp4
Gpc3
Sulf1
Bmpr1a
Fstl1
Smad5
Notch2
Neo1
Kdr
Wnt5a
Bmp6
Tgfbr3
Fbn1
Vsir
Smad2
Bmpr2
Usp9x
Hipk2
Sod2
Gpx3
Tldc2
Sesn3
Nqo1
Tnfaip3
Gpx8
Ercc2
Prdx4
Gclm
Gpx1
Prdx6
Sesn1
Prdx5
Ggt7
Idh2
Txn2
Ctrl-1
Ctrl-2
EP-1
EP-2

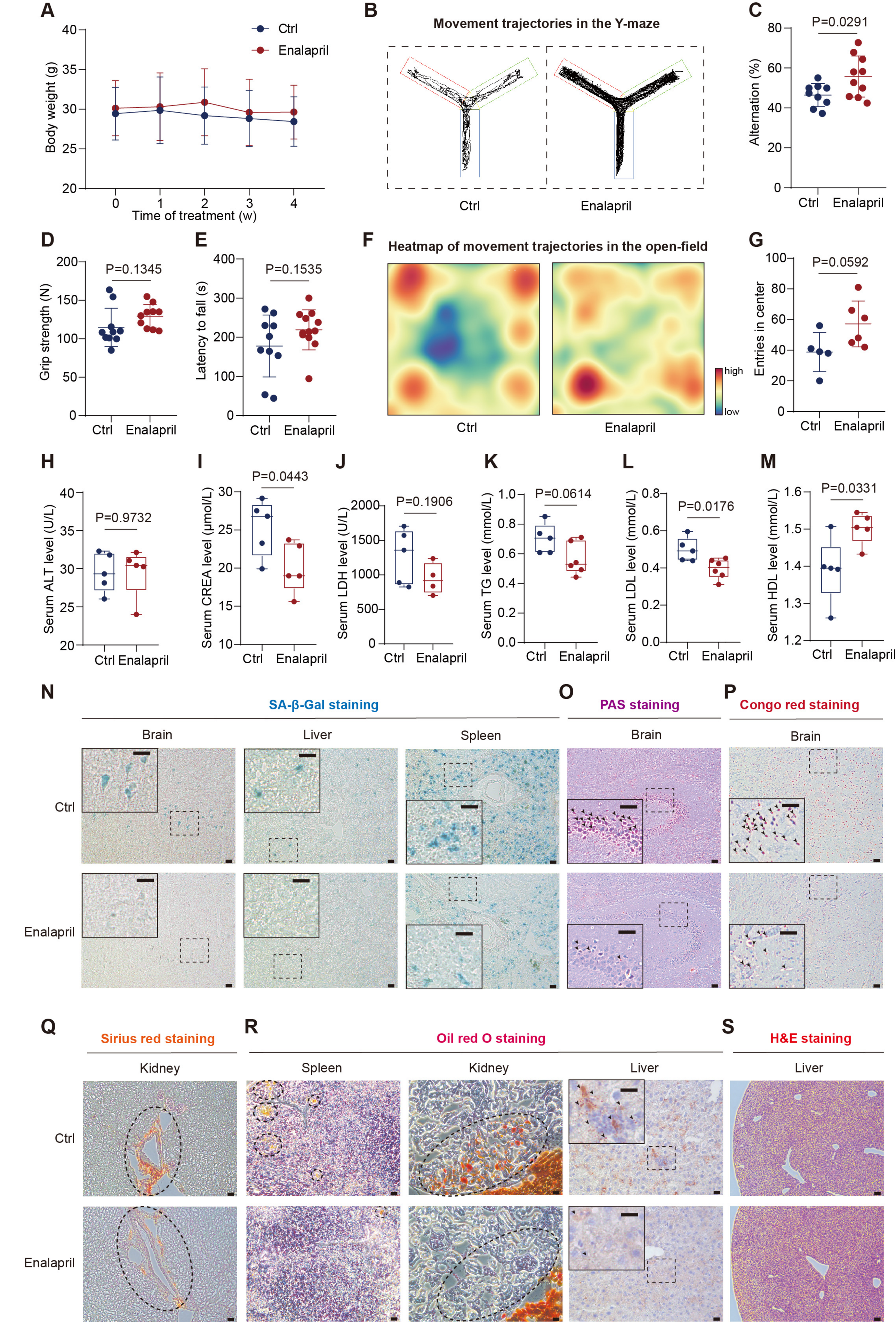
A
Ctrl
Enalapril
Body weight (g)
Time of treatment (w)
B
Movement trajectories in the Y-maze
Ctrl
Enalapril
C
P=0.0291
Alternation (%)
Ctrl
Enalapril
D
P=0.1345
Grip strength (N)
Ctrl
Enalapril
E
P=0.1535
Latency to fall (s)
Ctrl
Enalapril
F
Heatmap of movement trajectories in the open-field
high
low
Ctrl
Enalapril
G
P=0.0592
Entries in center
Ctrl
Enalapril
H
P=0.9732
Serum ALT level (U/L)
Ctrl Enalapril
I
P=0.0443
Serum CREA level (μmol/L)
Ctrl
Enalapril
J
P=0.1906
Serum LDH level (U/L)
Ctrl
Enalapril
K
P=0.0614
Serum TG level (mmol/L)
Ctrl
Enalapril
L
P=0.0176
Serum LDL level (mmol/L)
Ctrl
Enalapril
M
P=0.0331
Serum HDL level (mmol/L)
Ctrl
Enalapril
N
SA-β-Gal staining
Brain
Liver
Spleen
Ctrl
Enalapril
O
PAS staining
Brain
P
Congo red staining
Brain
Q
Sirius red staining
Kidney
Ctrl
Enalapril
R
Oil red O staining
Spleen
Kidney
Liver
Ctrl
Enalapril
S
H&E staining
Liver

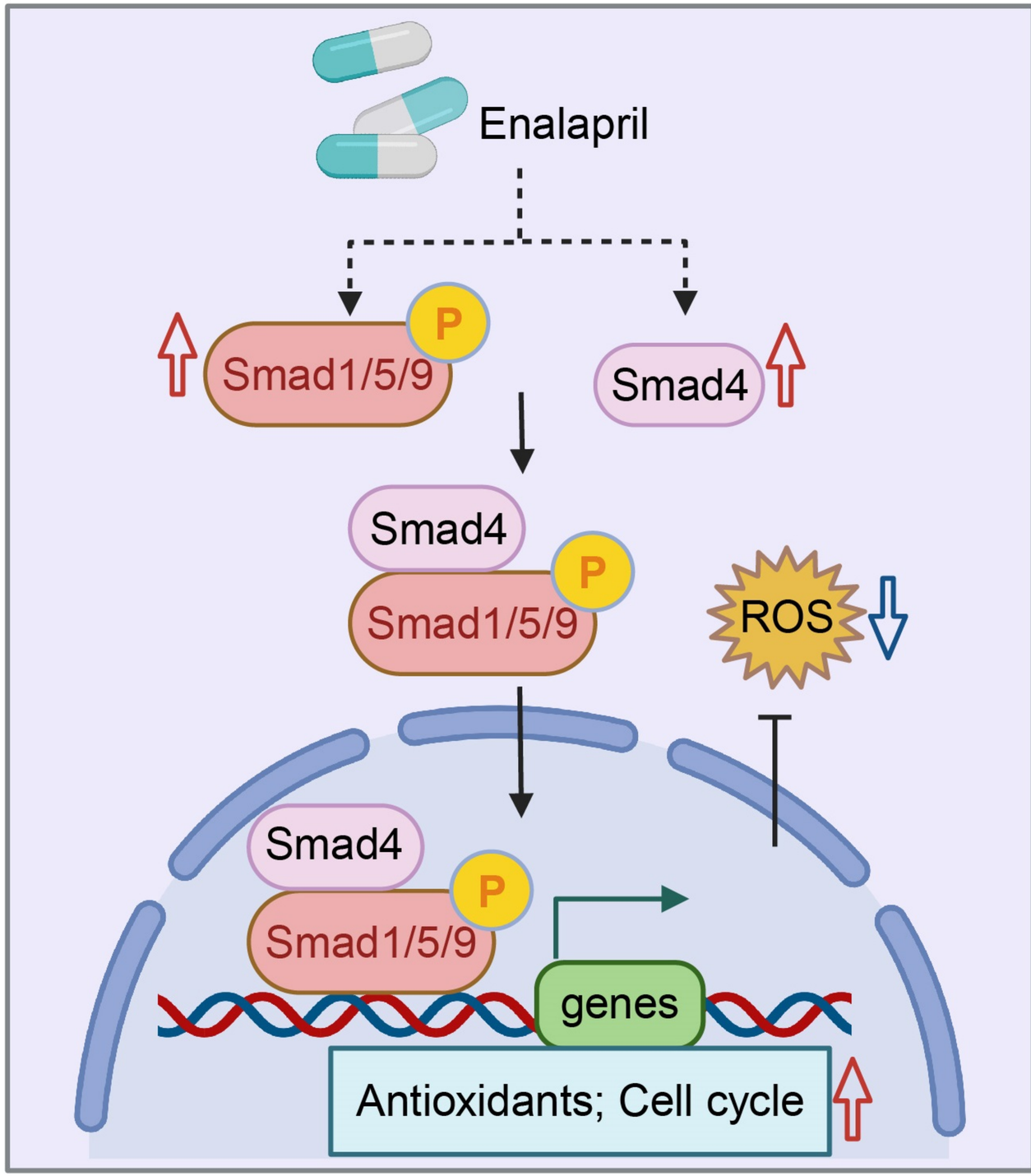
Enalapril
Smad1/5/9
P
Smad4
Smad4
Smad1/5/9
P
ROS
Smad4
Smad1/5/9
P
genes
Antioxidants; Cell cycle

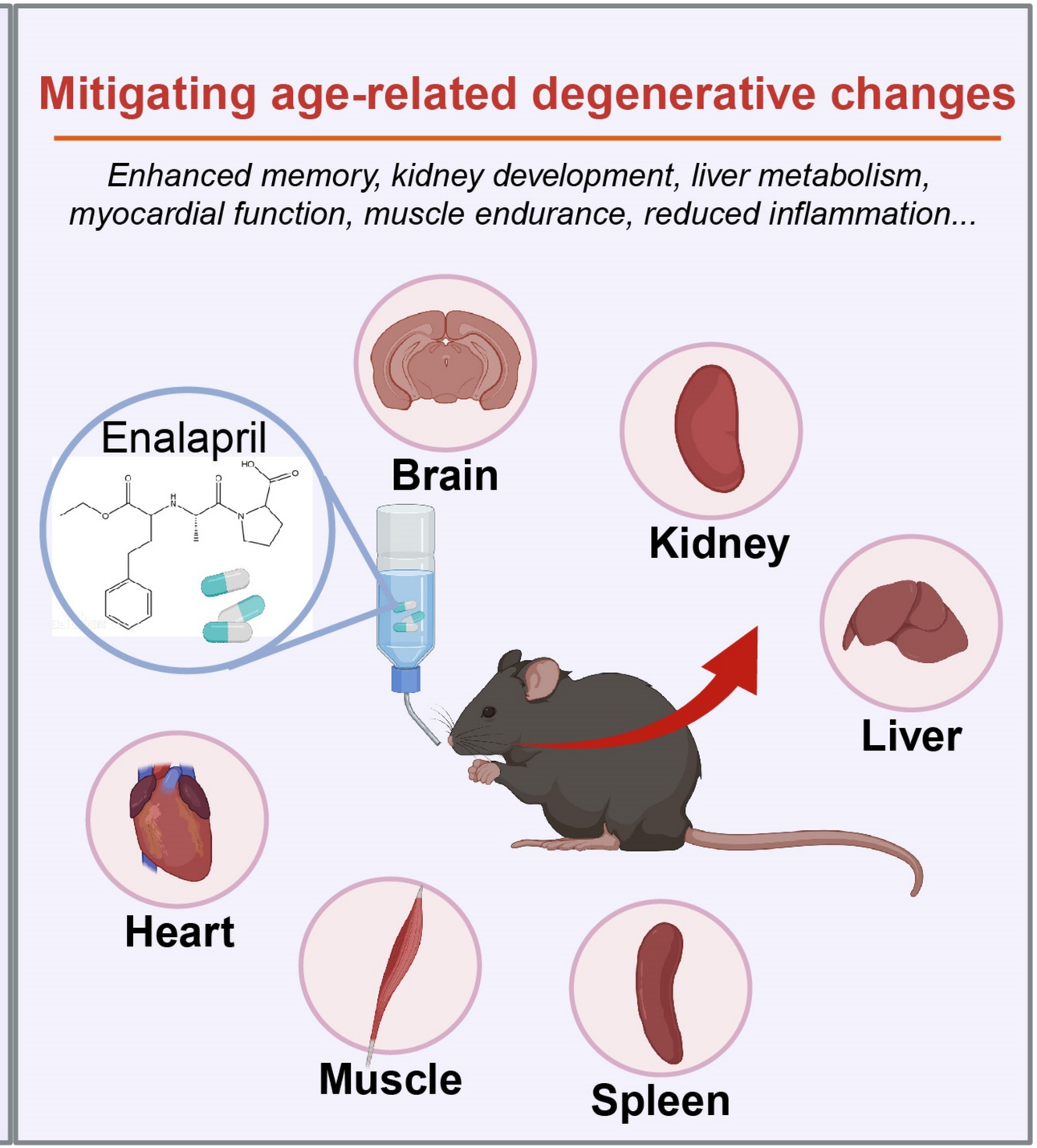
Mitigating age-related degenerative changes
Enhanced memory, kidney development, liver metabolism, myocardial function, muscle endurance, reduced inflammation...
Enalapril
Brain
Kidney
Liver
Heart
Muscle
Spleen